

**Hall transport in organic semiconductors**Michel Panhans  and Frank Ortmann *TUM School of Natural Sciences, Department of Chemistry, Technische Universität München, 85748 Garching b. München, Germany*

(Received 13 July 2023; revised 7 August 2024; accepted 19 August 2024; published 3 September 2024)

We establish a universal theory to understand quasiparticle Hall effects and transverse charge-carrier transport in organic semiconductors. The simulations are applied to organic crystals inspired by rubrene and cover multiple transport regimes. This includes calculations of the intrinsic Hall conductivity in pristine crystals, which are connected with a simple description of semiclassical electron transport that involves the concept of closed electronic orbits in the band structure, which can be easily calculated in density functional theory. Furthermore, this framework is employed to simulate temperature-dependent longitudinal and transverse mobilities in rubrene. These simulations are compared to experimental findings, providing insights into these results by characterizing the nonideality of the Hall effect due to the influence of vibrational disorder. We finally investigate the conditions for the observation of Shubnikov–de Haas oscillations in the longitudinal resistivity and quantized Hall plateaus in the transverse resistivity. A clear picture why this is not observed in rubrene is developed. These insights into classical and quantum Hall effects and their intermediates in organic semiconductors establish a blueprint for future explorations in similar systems.

DOI: [10.1103/PhysRevB.110.125202](https://doi.org/10.1103/PhysRevB.110.125202)**I. INTRODUCTION**

Investigating electronic transport by Hall measurements is of great interest for semiconductors and metals because Hall transport provides deep insights into the quasiparticle states, electron-transport mechanisms, and topological properties of band structures [1]. The universality and efficiency of a theoretical description of Hall transport is indicated by the seamless transition between quantum and classical regimes and its applicability to challenging systems, respectively. High-mobility organic semiconductors (OSCs) are such systems, for which the classical Hall effect has been reported in rubrene single-crystal organic field-effect transistors (OFETs) [2]. Subsequent Hall measurements in rubrene [3–10] at moderately low temperatures and several other systems [9,11–15] have been performed to study the nature of the charge carriers. A two-dimensional hole gas in C<sub>8</sub>-DNBDT-NW was measured down to temperatures around 10 K [16], in which the Hall mobilities indicate the existence of band transport. However, so far, no signature of a possible quantized Hall effect, like the integer quantum Hall effect (IQHE) [17–19], has been observed. The interest in the topological nature of these quantization phenomena, for which cryogenic temperatures lead to a step profile in the Hall resistance, opened a wide research field [17,19–22] but not yet in OSCs, where even numerical schemes for a quantitative description of Hall effects are only rarely reported in the literature [23,24]. Considering the breadth of experimental and theoretical developments of the Hall effect in various scientific contexts, its universal understanding covering all different facets including semiclassical band theories, Berry-phase physics [17,25], Boltzmann-transport approaches [26], transient theories involving carrier localization [27–29], and carrier hopping [30–32], etc. has not been established and seems out of reach.

In this work, we develop such a universal theory and study the dc-Hall effect using an efficient time-domain representation [33] for the electrical conductivity based on the general Kubo formula [33,34]. Within this quantum mechanical framework, we explicitly consider vibrational disorder arising from the electron-phonon coupling (EPC) to low-energy molecular vibrations. We study different Hall-transport regimes in rubrene by varying the strength of the disorder. While disorder can indeed vary in different experimental setups, our main purpose here is to generate more insights by this variation. First, we characterize the Hall conductivity for the states derived from the HOMO (highest occupied molecular orbital) of rubrene at vanishing disorder. By including vibrational disorder, we additionally investigate the temperature dependence of the Hall effect in bulk rubrene crystals and compare our results to experimental data. It is shown that, in the presence of vibrational disorder, different transport states must contribute to longitudinal and transverse charge transport in full agreement with experimental findings. In the presence of weak disorder, in general the Hall conductivity can become quantized due to the formation of Landau bands [35], which shows the topological nature of the Hall effect owing to the intrinsic Berry curvature [20,25,36,37]. We determine the conditions under which Hall plateaus in the transverse resistivity and Shubnikov–de Haas (SdH) oscillations in the channel resistivity can be observed and when they break down.

**II. THEORY****A. Hall-transport theory**

We first introduce the essential ingredients of the developed Hall-transport theory and the numerical methods employed, which are necessary for both the conceptual understanding of

Hall effects and for the practical evaluation of Hall responses in OSCs. The theoretical basis is a time-domain approach to study linear responses based on the Kubo formalism [33]. Within this framework, the electrical dc-conductivity tensor  $\sigma$  of effective noninteracting quasiparticles reads

$$\sigma_{\alpha\beta} = \frac{e^2}{2V} \int_0^\infty dt e^{-\frac{t}{\tau}} \int_{-\infty}^\infty dE \left[ -\frac{1}{2} \frac{df(E)}{dE} \frac{d^2}{dt^2} \mathcal{D}_{x_\alpha x_\beta}^+(E, t) + \frac{1}{\hbar} f(E) \frac{d}{dt} \mathcal{D}_{x_\alpha x_\beta}^-(E, t) \right], \quad (1)$$

with the Fermi function  $f(E) = (e^{\beta(E-\mu)} + 1)^{-1}$ , the (phenomenological) relaxation time  $\tau$ , and the correlation functions

$$\mathcal{D}_{x_\alpha x_\beta}^+(E, t) = \text{Tr}(\delta(E - \hat{H})\{\Delta\hat{x}_\alpha(t), \Delta\hat{x}_\beta(t)\}), \quad (2)$$

$$\mathcal{D}_{x_\alpha x_\beta}^-(E, t) = -i \text{Tr}(\delta(E - \hat{H})[\Delta\hat{x}_\alpha(t), \Delta\hat{x}_\beta(t)]), \quad (3)$$

in which the square brackets and the curly brackets denote the commutator and the anticommutator, respectively. The time evolution of  $\Delta\hat{x}_\alpha(t) = \hat{x}_\alpha(t) - \hat{x}_\alpha(0)$  for the Cartesian direction  $\alpha$  is driven by the Hamiltonian  $\hat{H}$ , describing effectively noninteracting quasiparticles (see Appendixes A and B for the detailed derivation). The symmetric and the antisymmetric parts of the conductivity tensor components  $\sigma_{\alpha\beta}^{\text{(as)}} = [\sigma_{\alpha\beta} + (-)\sigma_{\beta\alpha}]/2$  then read

$$\sigma_{\alpha\beta}^s = -\frac{e^2}{4V} \int_0^\infty dt e^{-\frac{t}{\tau}} \int_{-\infty}^\infty dE \frac{df(E)}{dE} \frac{d^2}{dt^2} \mathcal{D}_{x_\alpha x_\beta}^+(E, t), \quad (4)$$

$$\sigma_{\alpha\beta}^{\text{as}} = \frac{e^2}{2V\hbar} \int_0^\infty dt e^{-\frac{t}{\tau}} \int_{-\infty}^\infty dE f(E) \frac{d}{dt} \mathcal{D}_{x_\alpha x_\beta}^-(E, t). \quad (5)$$

The Hall conductivity is given by the antisymmetric part of the tensor, i.e.,  $\sigma_H = \sigma_{\alpha\beta}^{\text{as}}$ . Due to the general Onsager-Casimir relations [38–40] for the electrical conductivity  $\sigma_{\alpha\beta}(B_y) = \sigma_{\beta\alpha}(-B_y)$ , only the antisymmetric part  $\sigma_{\alpha\beta}^{\text{as}}$  describes a field-induced Hall voltage  $V_H = [V_H(B_y) - V_H(-B_y)]/2$ , while the symmetric part  $\sigma_{\alpha\beta}^s$  is invariant under reversal of the magnetic field. We numerically evaluate Eq. (1), using a linear-scaling quantum-transport approach [41], the Lanczos algorithm, and a Chebyshev expansion for the determination of the functions  $\mathcal{D}_{x_\alpha x_\beta}^\pm(E, t)$ . From the computed dc-conductivity tensor  $\sigma$ , we obtain the resistivity tensor by inversion,  $\rho = \sigma^{-1}$ .

## B. Relation to other Hall-transport theories

In this theoretical section, we shortly discuss how the present work includes other known Hall-transport approaches used in the past such as the description of the Hall conductivity in terms of the Berry curvature [20]. From the present approach starting from Eq. (1) (see Appendix D for details), we obtain the Hall conductivity as

$$\sigma_H = \frac{ie^2\hbar}{V} \sum_{mn} f(\varepsilon_n) \frac{(v_{nm}^\alpha v_{mn}^\beta - v_{nm}^\beta v_{mn}^\alpha)}{(\varepsilon_n - \varepsilon_m)^2 + \left(\frac{\hbar}{\tau}\right)^2}, \quad (6)$$

with  $v_{nm}^\alpha$  being the matrix elements of the velocity operator expanded in the quasiparticle eigenbasis of a proper quasiparticle Hamiltonian with eigenenergies  $\varepsilon_n$ . In the limit  $\tau \rightarrow \infty$ ,

the Hall conductivity is obtained from the thermally averaged Berry curvature, which is the key property in the theory of the IQHE.

For the symmetric part of the conductivity  $\sigma_{\alpha\beta}^s$ , we obtain from Eq. (1) (see Appendixes B and D) in the limit  $\tau \rightarrow \infty$

$$\sigma_{\alpha\beta}^s = \frac{\beta e^2 \pi \hbar}{2V} \sum_{mn} f(\varepsilon_n) [1 - f(\varepsilon_n)] \delta(\varepsilon_n - \varepsilon_m) \times (v_{nm}^\alpha v_{mn}^\beta + v_{nm}^\beta v_{mn}^\alpha). \quad (7)$$

For  $\alpha = \beta$ , this symmetric part becomes equivalent to the Kubo-Greenwood-type formula for longitudinal charge transport [41,42].

In addition, we prove in Appendix E that Eq. (1) is also equivalent to the Kubo-Bastin [43] formula and to the Kubo-Bastin-Strěda formula [44], which establishes additional exact relationships to other numerical schemes used to study charge transport in (topological) condensed matter systems [45–47]. More specifically, the Kubo-Bastin formula [43] describes the dc conductivity in the form

$$\sigma_{\alpha\beta} = \frac{e^2}{V} \int_{-\infty}^\infty dE f(E) C_{\alpha\beta}(E), \quad (8)$$

with the correlation function

$$C_{\alpha\beta}(E) = i\hbar \text{Tr} \left[ \hat{v}_\alpha \delta(E - \hat{H}) \hat{v}_\beta \frac{d\hat{G}^+(E)}{dE} - \text{H.c.} \right], \quad (9)$$

which depends on the one-particle Green's function operator  $\hat{G}^\pm(E) = \lim_{\eta \rightarrow 0} (E - \hat{H} \pm i\eta)^{-1}$ . The equivalence of Eq. (1) with the Kubo-Bastin and the Kubo-Bastin-Strěda formula is obtained from the decomposition of the correlation function  $C_{\alpha\beta}(E)$  into symmetric and antisymmetric parts  $C_{\alpha\beta}^{\text{(as)}}(E) = [C_{\alpha\beta}(E) + (-)C_{\beta\alpha}(E)]/2$  yielding

$$C_{\alpha\beta}^s(E) = \pi\hbar \frac{d}{dE} \text{Tr}[\delta(E - \hat{H}) \hat{v}_\alpha \delta(E - \hat{H}) \hat{v}_\beta], \quad (10)$$

$$C_{\alpha\beta}^{\text{as}}(E) = i\hbar \text{Tr} \left[ \delta(E - \hat{H}) \left( \hat{v}_\alpha \frac{1}{(E - \hat{H})^2} \hat{v}_\beta - \text{H.c.} \right) \right]. \quad (11)$$

From this decomposition, we obtain the same result for  $\sigma_{\alpha\beta}^s$  and  $\sigma_H$  as derived from Eq. (1) and thus demonstrate the equivalence to the Kubo-Bastin formula in Eq. (8) (see Appendixes D and E for details). To compare Eq. (1) with the Kubo-Bastin-Strěda formula, the Hall conductivity is decomposed into two terms  $\sigma_H = \sigma_H^I + \sigma_H^{II}$ , where  $\sigma_H^{II}$  is given by

$$\sigma_H^{II} = \frac{e^2}{2V} \int_{-\infty}^\infty dE f(E) \text{Tr} \left[ \frac{d}{dE} \delta(E - \hat{H}) (\hat{x}_\alpha \hat{v}_\beta - \hat{x}_\beta \hat{v}_\alpha) \right], \quad (12)$$

which explicitly appears in the Strěda formula and has previously been used to explain the quantization of the Hall conductivity [44]. This contribution to the Hall conductivity is also relevant to explain the intrinsic Hall conductivity in the disorder-free case (see below) and thus is, interestingly, at the origin of the semiclassical version of the Hall conductivity discussed in Sec. III A.

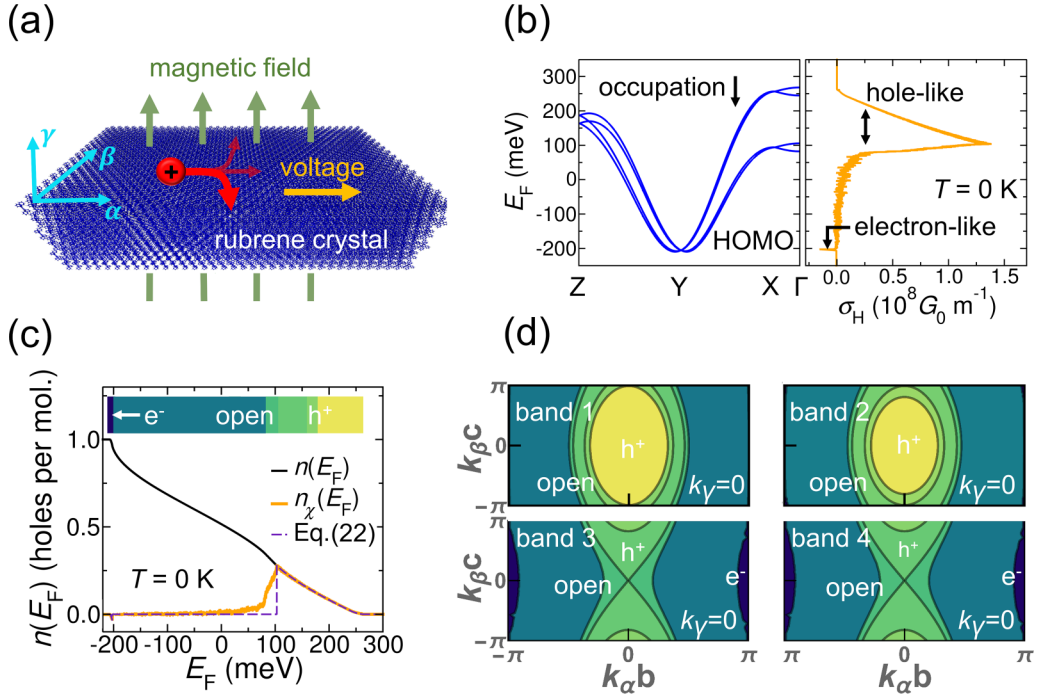


FIG. 1. Hall effect in rubrene at vanishing disorder. (a) Hall setup for bulk crystals, where a homogeneous magnetic field is applied perpendicular to the herringbone plane ( $\alpha\beta$  plane). (b) (Left panel) Band structure of the four HOMO bands. (Right panel) Energy-resolved Hall conductivity  $\sigma_H$  at 0 K. The axes are flipped ( $\sigma_H \leftrightarrow E_F$ ) to compare both panels more easily. (c) Energy-resolved density  $n_\chi$  at 0 K. The total charge-carrier concentration  $n$  (black) and the analytical result from Eq. (22) (dashed indigo line) are plotted for comparison. The colored bar in the inset defines different regimes and their energy separation. (d) Contour plot of the Fermi surface at  $k_\gamma = 0$  for all four bands at different energies. The contour lines are defined by energies of the colored bar in (c). Holelike, electronlike, and open-orbit domains are indicated.

In addition to covering previous theories, Eq. (1) provides us with the full quantum-dynamical time evolution of the involved transport correlation functions. This permits investigating any transport regime, which otherwise demands conceptually different theories used previously. It also offers detailed information on, e.g., the formation of topological states on the time scale of localization and scattering effects.

### C. Effective quasiparticle Hamiltonian and simulation geometry for rubrene

We study the Hall effect for a three-dimensional rubrene crystal with lateral dimensions of  $0.06 \mu\text{m} \times 0.8 \mu\text{m} \times 1.6 \mu\text{m}$ , including around  $10^8$  coupled hole orbitals. We focus on the HOMO-derived states as an example, as holes are the usual carrier type in rubrene and similar OSCs. In this setup, the  $\alpha$  direction [see Fig. 1(a)] is aligned with the high-mobility direction of the rubrene crystal, while the  $\beta$  direction is perpendicular to  $\alpha$  and lies also inside the herringbone plane. The lattice parameters of the crystal are given by  $a = 26.789 \text{ \AA}$  ( $\gamma$  direction),  $b = 7.170 \text{ \AA}$  ( $\alpha$  direction; see Fig. 1), and  $c = 14.211 \text{ \AA}$  ( $\beta$  direction) of an orthorhombic Bravais lattice and are taken from the literature [48]. The four rubrene molecules arrange in a herringbone structure in the  $\alpha\beta$  plane with the center-of-mass coordinates  $A = (0, 0, 0)$ ,  $B = (\frac{a}{2}, 0, \frac{c}{2})$ ,  $C = (0, \frac{b}{2}, \frac{c}{2})$ , and  $D = (\frac{a}{2}, \frac{b}{2}, 0)$ . A suitable tight-binding expression for the four bare electronic bands with a minimal number

of electronic transfer integrals reads

$$\begin{aligned} \varepsilon(\mathbf{k}, \pm, \pm) &= 2\varepsilon_{AA+b} \cos(k_\alpha b) + 2\varepsilon_{AA+2b} \cos(2k_\alpha b) \\ &\pm 4\varepsilon_{AC} \cos\left(\frac{k_\alpha b}{2}\right) \cos\left(\frac{k_\beta c}{2}\right) \\ &\pm 4\varepsilon_{AB} \cos\left(\frac{k_\gamma a}{2}\right) \cos\left(\frac{k_\alpha b}{2}\right), \end{aligned} \quad (13)$$

with the transfer integrals  $\varepsilon_{ij}$  taken from prior work [48].

To model hole transport in rubrene crystals, these parameters enter a Hamiltonian of the form

$$\hat{H} = \sum_{i,j} e^{-i\varphi_{ij}} \tilde{P} [\varepsilon_{ij} + V_{ij}(T)] \hat{c}_i^\dagger \hat{c}_j + \sum_i V_{ii}(T) \hat{c}_i^\dagger \hat{c}_i, \quad (14)$$

which is derived from a Holstein-Peierls Hamiltonian. Equation (14) includes, besides the above  $\varepsilon_{ij}$  between the molecular orbitals, an effective description of the EPC, where the matrix elements  $V_{ii}(T)$  and  $V_{ij}(T)$  (see below) describe a temperature-dependent vibrational disorder potential caused by the coupling to low-energy vibrational modes. It also includes a polaron renormalization factor  $\tilde{P}$  caused by the coupling to high-energy vibrational modes (see Refs. [29,49–51] for details). The Peierls phase  $\varphi_{ij}$  [52] describes the interaction of the holes with a homogeneous magnetic field and is generically defined as [52]

$$\varphi_{ij} = \frac{e}{\hbar} \int_{\mathbf{r}_i}^{\mathbf{r}_j} \mathbf{d}\mathbf{r} \cdot \mathbf{A}(\mathbf{r}), \quad (15)$$

with the vector potential  $\mathbf{A}(\mathbf{r}) = Bx_\beta \mathbf{e}_\alpha + B'x_\alpha \mathbf{e}_\beta$  and the resulting magnetic field  $\mathbf{B} = B_\gamma \mathbf{e}_\gamma$  with the constant amplitude  $B_\gamma = B - B'$ . The contributions to the model Hamiltonian that arise from EPC are given by (see, e.g., Ref. [51])

$$V_{ij}(T) = \sum_\lambda \hbar\omega_\lambda g_{ij}^\lambda \sqrt{1 + 2n_\lambda} \left( \frac{\phi_i^\lambda + \phi_j^\lambda}{2} \right), \quad (16)$$

$$\tilde{P} = e^{-\sum_\xi (g_{ii}^\xi)^2 (1+2n_\xi)}. \quad (17)$$

Here,  $\phi_i$  are Gaussian random numbers describing the vibrational disorder of low-energy modes, which arises from tracing out these degrees of freedom.  $\hbar\omega_\lambda$  and  $\hbar\omega_\xi$  are the vibrational mode energies of the low-energy and high-energy modes, respectively.  $n_\lambda = 1/(e^{\beta\hbar\omega_\lambda} - 1)$  and  $n_\xi$  (defined accordingly) are their thermal occupations, while  $g_{ij}^\lambda$  and  $g_{ij}^\xi$  are the respective coupling constants to the electronic states. The vibrational disorder is based on *ab initio* material parameters taken from Ref. [48] and is a static Gaussian disorder, which modifies the on-site energies  $\varepsilon_{ii}$  and the transfer integrals  $\varepsilon_{ij} \in \{\varepsilon_{AA+b}, \varepsilon_{AA+2b}, \varepsilon_{AB}, \varepsilon_{AC}\}$  of the rubrene crystal. The mean strength of the vibrational disorder  $V_{ij}(T)$  is determined by its standard deviation averaged over all HOMO states, which is obtained from the EPC material parameters as

$$V_{\text{EPC}}^2(T) = \sum_\lambda (\hbar\omega_\lambda)^2 (1 + 2n_\lambda) \left[ (g_{ii}^\lambda)^2 + \frac{1}{2} \sum_{j \neq i} g_{ij}^\lambda g_{ji}^\lambda \right]$$

$$= V_0^2(T) + V_{AA+b}^2(T) + V_{AA+2b}^2(T) + 2V_{AC}^2(T) + 2V_{AB}^2(T), \quad (18)$$

where the sum over  $j$  only runs over the next neighbors of  $i$  with respect to the corresponding transfer integral. The sum over  $\lambda$  only includes low-frequency modes below a mode energy of 75 meV. The temperature dependence of the vibrational disorder potential is codetermined by the thermal occupation  $n_\lambda$  of mode  $\lambda$ .

In Table I (Appendix F), we summarize the energy parameters used in the effective polaron model in Eq. (14). We note that the value for  $V_{AA+2b}(T)$  is set to zero since the EPC constants  $g_{AA+2b}^\lambda$  have not been considered in Ref. [48] for the second-neighbor transfer integral  $\varepsilon_{AA+2b}$ . From Table I, we see that the vibrational disorder is dominated by the intramolecular contribution  $V_0(T)$  and has a total disorder strength of  $V_{\text{EPC}}^{300\text{K}} = 57.5$  meV. The polaron renormalization  $\tilde{P}$  obtained from the remaining high-frequency modes is evaluated to  $\tilde{P} = 0.72$ , which reduces the transfer integrals and the intermolecular vibrational disorder.

Finally, the cyclotron energy close to the HOMO band edge reads  $\hbar\omega_{\text{cyc}} = \hbar e B_\gamma / m_{\text{cyc}}$  with the inverse cyclotron mass

$$m_{\text{cyc}}^{-1} = \frac{\tilde{P}bc}{\hbar^2} \sqrt{\varepsilon_{AC}(2\varepsilon_{AA+b} + 8\varepsilon_{AA+2b} + \varepsilon_{AC} + \varepsilon_{AB})}, \quad (19)$$

which is derived from the pristine (but renormalized) HOMO band structure in Eq. (13). The cyclotron energy near the HOMO band edge amounts to 0.51 (5.1) meV for a magnetic field strength of 6 T (60 T).

The results derived from the proposed theoretical framework in Sec. III below, which encompasses investigations of three transport scenarios, illustrate distinct regimes of Hall

transport. These include semiclassical, quantum, topological, and localization effects, all integrated within a single framework. There, to illustrate the seamless transition between these regimes, we vary the EPC-induced disorder strength from zero to its full material-parameter-based values.

### III. RESULTS

#### A. Intrinsic Hall conductivity

The first Hall-transport scenario is the intrinsic limit of vanishing disorder, where we focus only on the Hall-transport properties stemming from the HOMO-band structure. In this first scenario, the coupling to low-energy vibrations, i.e., the vibrational disorder, is neglected, while the coupling to high-energy vibrations is included via a polaron renormalization factor of  $\tilde{P} = 0.72$ . We numerically evaluate the conductivity tensor in the herringbone plane [ $\alpha\beta$  plane; see Fig. 1(a)] and calculate the Hall conductivity  $\sigma_H$  at a magnetic field strength of  $B_\gamma = 6$  T, which is a typical modest value used in experiments. In Fig. 1(b) (right panel), the energy-resolved Hall conductivity (at 0 K for simplicity) is compared to the pristine band structure of the four HOMO bands [left panel in Fig. 1(b)] in rubrene bulk crystals. The results show an intrinsic Hall effect in the absence of disorder, which we now analyze in more detail.

We make two major observations. (i) The Hall conductivity is monotonically increasing from the top of the HOMO band around  $E_F = 250$  meV. However, this trend persists only down to a Fermi energy of around 100 meV. In this energy region, it shows a clear holelike behavior, where the magnetic-field response agrees with the usual right-hand rule [see Fig. 1(a)] as described by a fully classical model of the Hall effect. At lower energy ( $E_F \leq 100$  meV),  $\sigma_H$  drops rapidly to zero or turns even negative, which cannot be explained by a reasonable classical model and requires a quantum mechanical description. (ii) Despite the absence of disorder in the present scenario, one cannot observe any quantization effect in  $\sigma_H$  even at  $T = 0$  K.

To understand these observations and the distinct energy dependence of the Hall conductivity in Fig. 1(b), we analyze it by relating  $\sigma_H$  to the total carrier concentration  $n$  to quantify the number of hole states that contribute to the Hall effect. We thus define the density  $n_\chi$  that is characteristic for  $\sigma_H$  according to

$$en_\chi = \sigma_H B_\gamma. \quad (20)$$

$n_\chi$  is compared to the total carrier concentration  $n$  in Fig. 1(c). This shows that at low concentrations  $n_\chi$  agrees with  $n$  for  $E_F \geq 103$  meV (or  $n \leq 0.28$  holes per molecule). In addition, we find that, for  $n \leq 0.28$ ,  $en_\chi$  is also equal to the Hall density  $en_H$ , which implies  $n_H = n_\chi = n$  and thus describes an ideal Drude-like Hall effect ( $n_H = n$ ) of the holes with a Hall resistance of  $\rho_H = \sigma_H^{-1}$ . At lower Fermi energy,  $n_\chi$  decreases rapidly (between  $80 \text{ meV} \leq E_F \leq 100 \text{ meV}$ ) and almost vanishes for even lower energies. Since we do not observe any quantization effects in  $\sigma_H$  and  $\rho_H$ , we conclude that the obtained energy dependence of the Hall conductivity is an intrinsic property of the pristine band structure and should coincide with a semiclassical electron-transport theory [53].

Motivated by these numerical findings and going beyond the specific rubrene crystals, we have derived a simple and

general analytic expression for the intrinsic Hall conductivity from the full quantum description in Eq. (1). In absence of disorder and for a purely two-dimensional system (taken for simplicity), the intrinsic Hall conductivity yields the semiclassical expression

$$\sigma_{\text{H}}^{\text{sc}} = \frac{eN}{B_{\gamma}V} \int_{-\infty}^{\infty} dE f(E) \frac{d}{dE} \frac{A_e(E) - A_h(E)}{\Omega_{\text{BZ}}}. \quad (21)$$

This result involves the area difference  $A_e(E) - A_h(E)$  enclosed by all semiclassical quasiparticle orbits (both electron- and holelike) at energy  $E$  in the Brillouin zone (BZ).  $\sigma_{\text{H}}^{\text{sc}}$  furthermore depends on the total number of electronic states  $N$ , the chemical potential  $\mu$ , while  $\Omega_{\text{BZ}}$  is the BZ volume (see Appendix C for details of this derivation). For the particular case of rubrene, the Hall conductivity at zero temperature can further be approximated from Eq. (21) as

$$\sigma_{\text{H}} = \frac{e}{B_{\gamma}} \{n[1 - \Theta(E_{\text{F}} - E_h)] - n_e \Theta(E_{\text{F}} - E_e)\}, \quad (22)$$

with the Heaviside step function  $\Theta(E)$ . The energies  $E_h \approx 103$  meV and  $E_e \approx -202$  meV are introduced as the critical energies that separate energy domains where the Fermi surface describes closed holelike and electronlike orbits. Figure 1(d) illustrates these orbits as contours for  $k_{\gamma} = 0$ . Equation (22) describes the fact that for a Fermi energy of  $E_{\text{F}} > E_h$  an ideal holelike Hall effect is observed, i.e.,  $\sigma_{\text{H}} = en/B_{\gamma}$ , and for  $E_{\text{F}} < E_e$  an ideal electronlike Hall effect, i.e.,  $\sigma_{\text{H}} = -en_e/B_{\gamma}$  (with the electron concentration  $n_e = 1 - n$ ), is observed. For  $E_e < E_{\text{F}} < E_h$  the Hall conductivity vanishes. This is because the orbits are open in full agreement with the numerical results of  $en_{\chi}$  in Fig. 1(c). The closure of the orbits with changing energy can be seen in Fig. 1(d).

At this point we should emphasize the quality of these findings. Within the full quantum-mechanical treatment of  $\sigma_{\text{H}}$  (including the possible topological nature of the Hall conductivity) we have shown here that, in the absence of quantization phenomena and under conditions of sufficiently low disorder, the intrinsic Hall conductivity can be effectively explained. This explanation relies exclusively on analyzing the semiclassical orbits within the pristine band structure of the specified material (at zero magnetic field). This picture also captures transitions between ideal and nonideal Hall effects. Moreover, we find that the absence of quantization of the Hall conductivity is due to the relatively small energy spacing of the Landau bands at moderate fields of  $B_{\gamma} = 6$  T. The level spacing is competing with the band dispersion along the direction of the magnetic field, which is larger in the present case. This establishes the conditions under which such semiclassical responses may arise. We finally note that Eq. (21) can also be derived by assuming *a priori* a semiclassical regime of the Hall effect [54,55]. It is closely related to the presence of Lifshitz transitions [56] in the pristine band structure describing changes in the topology of the Fermi surface when changing the Fermi energy. Thus we find this regime to be a part of the present and more general Kubo approach.

## B. Temperature-dependent Hall effect in bulk rubrene crystals

We continue our analysis of the Hall effect in rubrene by studying its temperature dependence at a magnetic-field

strength of 6 T. In addition to Sec. III A, we now include the vibrational disorder based on our molecular parameters for the EPC in rubrene. To characterize the present Hall-transport regime, we calculate the Hall mobility  $\mu_{\text{H}}$ , the channel mobility  $\mu$ , and the Hall density  $en_{\text{H}}$ , which can be measured in Hall probes. More explicitly, these quantities are obtained from the resistivity components, yielding

$$\mu_{\text{H}} = \frac{\rho_{\alpha\alpha}}{B_{\gamma}\rho_{\text{H}}}, \quad \mu = \frac{1}{en\rho_{\alpha\alpha}}, \quad en_{\text{H}} = \frac{B_{\gamma}}{\rho_{\text{H}}}, \quad (23)$$

where  $\rho_{\alpha\alpha} = \rho$  is the resistivity along the high-mobility direction and  $\rho_{\text{H}}$  is the Hall resistance along the  $\beta$  direction [see Fig. 1(a) for comparison]. The resistivities  $\rho_{\alpha\alpha}$  and  $\rho_{\text{H}}$  are obtained from inversion of the full dc-conductivity tensor obtained from Eq. (1).

To get detailed insights into this Hall-transport regime, we analyze the dependencies of  $\mu_{\text{H}}$  and  $\mu$  on the relaxation time  $\tau$  and on the carrier concentration  $n$ . In Fig. 2(a), we plot the Hall mobility as a function of  $\tau$ , which turns out to be almost constant for  $\tau \geq 50$  fs and varies only slightly with temperature. On the other hand, the channel mobility  $\mu$  in Fig. 2(c) has a stronger dependence on  $\tau$  and decays at larger times. Note that large  $\tau$  can be associated to weaker external relaxation effects. This decay with  $\tau$  is a consequence of the vibrational disorder entering the Hamiltonian in Eq. (14) and leading to carrier localization, due to multiple scattering, at time scales of around 100 fs to 200 fs in agreement with the time scale of transient localization [27,29] in the absence of magnetic fields. This dependence suggests that the transport states contributing to the channel mobility become localized for intermediate times  $\tau$  and only the more extended transport states survive at larger times. In stark contrast, these localization effects for  $\mu$  are not found in  $\mu_{\text{H}}$ . This means that vibrational disorder has a smaller effect on those transport states that respond to the magnetic field by deflection, which is in full agreement with experimental findings [2] (see below).

Furthermore, we show in Figs. 2(b) and 2(d) that the mobilities for a fixed value of  $\tau$  do not vary significantly with the carrier concentration  $n$  at least for  $n \leq 10^{-2}$  that are achievable experimentally. That is, the transport characteristics are quite homogeneous at the top of the HOMO band and therefore should not depend much on the gate voltage.

To finally compare our results, characterized by a distinct time and concentration dependence, to experimental data, for which this information is not directly available, one needs to fix certain values for  $\tau$  and  $n$ . For the carrier concentration, we use  $n = 2.5 \times 10^{-4}$  holes per molecule, which is similar to the experimental value of roughly  $10^{10}$  cm $^{-2}$  and which has already been used to calculate the mobilities shown in Figs. 2(a) and 2(c). To fix the relaxation time  $\tau$ , we match the numerically calculated value of the ratio  $\mu/\mu_{\text{H}} \equiv n_{\text{H}}/n$  with the experimental ratio  $\mu^{\text{expt}}/\mu_{\text{H}}^{\text{expt}} \equiv n_{\text{H}}^{\text{expt}}/n^{\text{expt}}$  of Ref. [2] [cf. Fig. 3(d)]. This is possible because of the consistency of experimental and theoretical results. More specifically, we find in Fig. 3(a) that  $n_{\text{H}}/n$  also decays over time at fixed  $n$  and is almost constant in the entire HOMO band at fixed  $\tau$  [see Fig. 3(b)]. Therefore, equating the mobility ratios yields the relaxation times as indicated by circles in Fig. 3(a). We find that the resulting transport time scales, ranging from 50 fs at 300 K to 250 fs at 180 K, are consistent with the

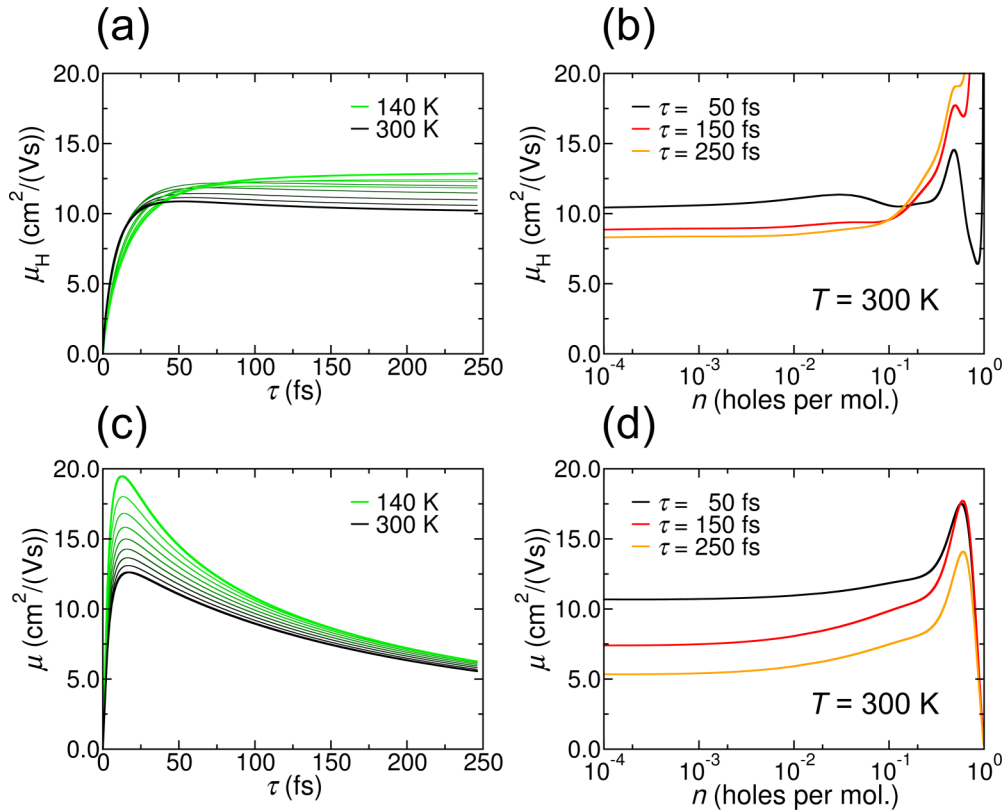


FIG. 2. Temperature-dependent Hall transport in bulk rubrene crystals at 6 T. (a), (c) Time dependence of the Hall mobility and the channel mobility for temperatures between 140 K and 300 K in steps of 20 K. (b), (d) Concentration dependence of the Hall mobility and channel mobility for fixed  $\tau$  of 50 fs, 150 fs, and 250 fs at 300 K. In (a) and (c), the carrier concentration is fixed to  $n = 2.5 \times 10^{-4}$  holes per molecule.

transport time scale within transient localization theory [27]. In contrast to transient localization theory, in which  $\tau$  is related to characteristic time scales of low-energy vibrations, the value of  $\tau$  is here determined from the comparison of the experimental and the theoretical Hall density, fixing  $\tau$  as a free parameter. We emphasize that this is not a contradiction to transient localization theory since the present values of  $\tau$  are smaller than the typical time scale of low-energy vibration modes, which is the upper limit of the time scale where the vibrational-disorder model is a valid treatment of the EPC.

Based on the fixed values for  $n$  and  $\tau$ , we calculate the temperature-dependent mobilities shown in Fig. 3(c). For comparison, Fig. 3(d) shows the experimental Hall measurement carried out by Podzorov *et al.* [2] on vacuum-gated rubrene single-crystal OFETs. Both theoretical and experimental results agree in that Hall and channel mobilities are equal at room temperature but differ at lower temperatures according to  $\mu_H > \mu$ . This indicates the formation of localized carriers due to vibrational disorder at low  $T$ . We note that the temperature dependence of the channel mobility  $\mu$  in Fig. 3(c) especially its downturn towards lower temperatures [with  $d\mu(T)/dT > 0$ ] is a direct consequence of the treatment of the EPC as vibrational disorder within the transient localization approach. Given that the validity of transient localization is limited to transport time scales of up to a few hundred femtoseconds and may not extend to the lowest temperatures, we there also consider different predicted mobility behaviors. For instance, in diagrammatic

Monte Carlo-based approaches without an assumed relaxation time, it was suggested that an activated temperature dependence [ $d\mu(T)/dT > 0$ ] at low temperatures only occurs at elevated EPC values [57,58]. This suggests a possible limitation of transient localization theory, at least for studied models that involve a single high-frequency vibration mode and a single charge carrier in a one-dimensional model crystal. However, a more detailed comparison is clearly beyond the scope of this work. In general, the theoretical results are in good qualitative agreement to experimental mobility values; still we note that also static disorder caused, e.g., by surface disorder or impurities might lead to a mobility downturn due to carrier localization.

We note that the difference between the channel and Hall mobilities has been explained previously with a phenomenological model put forward by Yi *et al.* [7]. In this model, the difference is attributed to the presence of two distinct types of charge carriers: bandlike carriers and hopping carriers, the latter of which do not respond to the magnetic field. Different to this minimal semiclassical model, in our approach all types of transport states and all of their potential coherent interferences are naturally included. An attempt was made to apply such phenomenological models for illustration, but the results were not satisfactory, which might be due to the absence of clearly distinct types of carriers or the effect of multiple scattering and localization. Instead, the understanding of the Hall transport in rubrene can be enhanced by analyzing the density  $n_\chi = \sigma_H B_y$  defined in Eq. (20) and connect the present

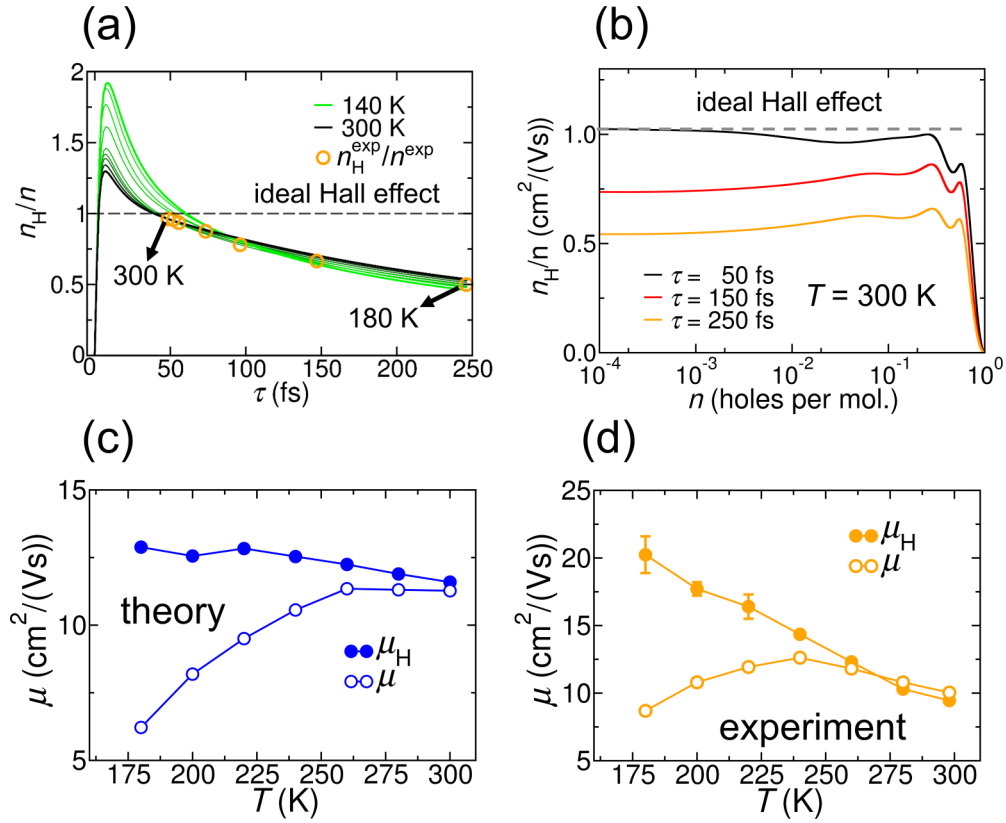


FIG. 3. Temperature-dependent Hall transport in bulk rubrene crystals at 6 T. (a) Time dependence of the Hall density for temperatures between 140 K and 300 K in steps of 20 K. (b) Concentration dependence of the Hall density for fixed  $\tau$  of 50 fs, 150 fs, and 250 fs at 300 K. In (a) the orange circles indicate the experimental reference values obtained in Ref. [2]. The gray dashed lines in (a) and (b) indicate the equality between the carrier density and the Hall density  $n = n_H$ . (c) Theoretical Hall and channel mobilities. (d) Experimental Hall and channel mobilities taken from Ref. [2].

Hall-transport regime to the intrinsic disorder-free case discussed above (Sec. III A). Specifically, for  $n_\chi$  we find similar dependencies on the carrier concentration  $n$  and on  $\tau$  with its decay over time (cf. Fig. 4). For a fixed value of  $\tau$ , the ratio  $n_\chi/n$  changes only weakly in the entire HOMO band, which is similar to  $\mu_H$ ,  $\mu$ , and  $n_H/n$ . This result indicates that the number of states that respond to the magnetic field also increases uniformly with  $n$  for carrier concentrations up to  $10^{-1}$ . The difference to the intrinsic case discussed earlier,

however, is very pronounced and eventually quite insightful. While the Hall density  $n_H$ , both in the disorder-free and in the disordered case, is of the order of the carrier concentration  $n_H \approx n$  (see above), the density  $n_\chi$  is now five orders of magnitude smaller than  $n$ . This behavior is totally different to the pristine case, where we found  $n_\chi \approx n$  for  $n \leq 0.28$  holes per molecule, which we attributed to the distribution of holelike, electronlike, and open orbits in the HOMO band of rubrene [see discussion of Fig. 1(c)]. In stark contrast here, the

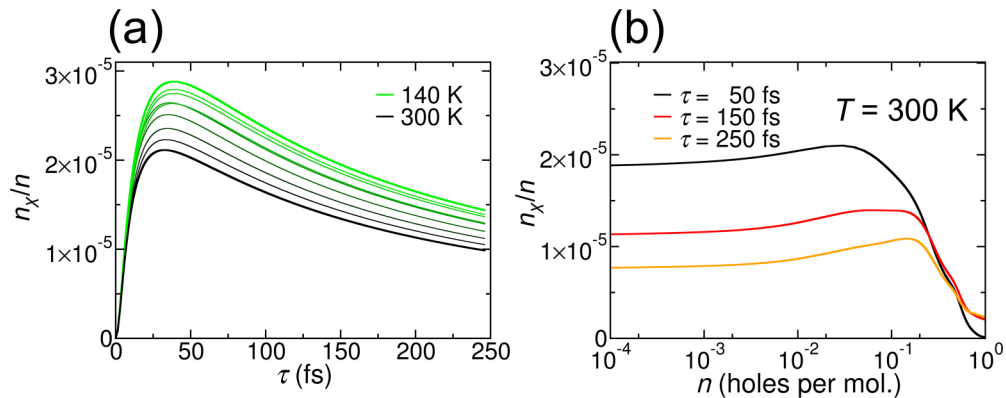


FIG. 4. Time and concentration dependence of  $n_\chi$ . (a) Time dependence of the density  $n_\chi$  for temperatures between 140 K and 300 K in steps of 20 K. (b) Concentration dependence of the density  $n_\chi$  for fixed  $\tau$  of 50 fs, 150 fs, and 250 fs at 300 K.

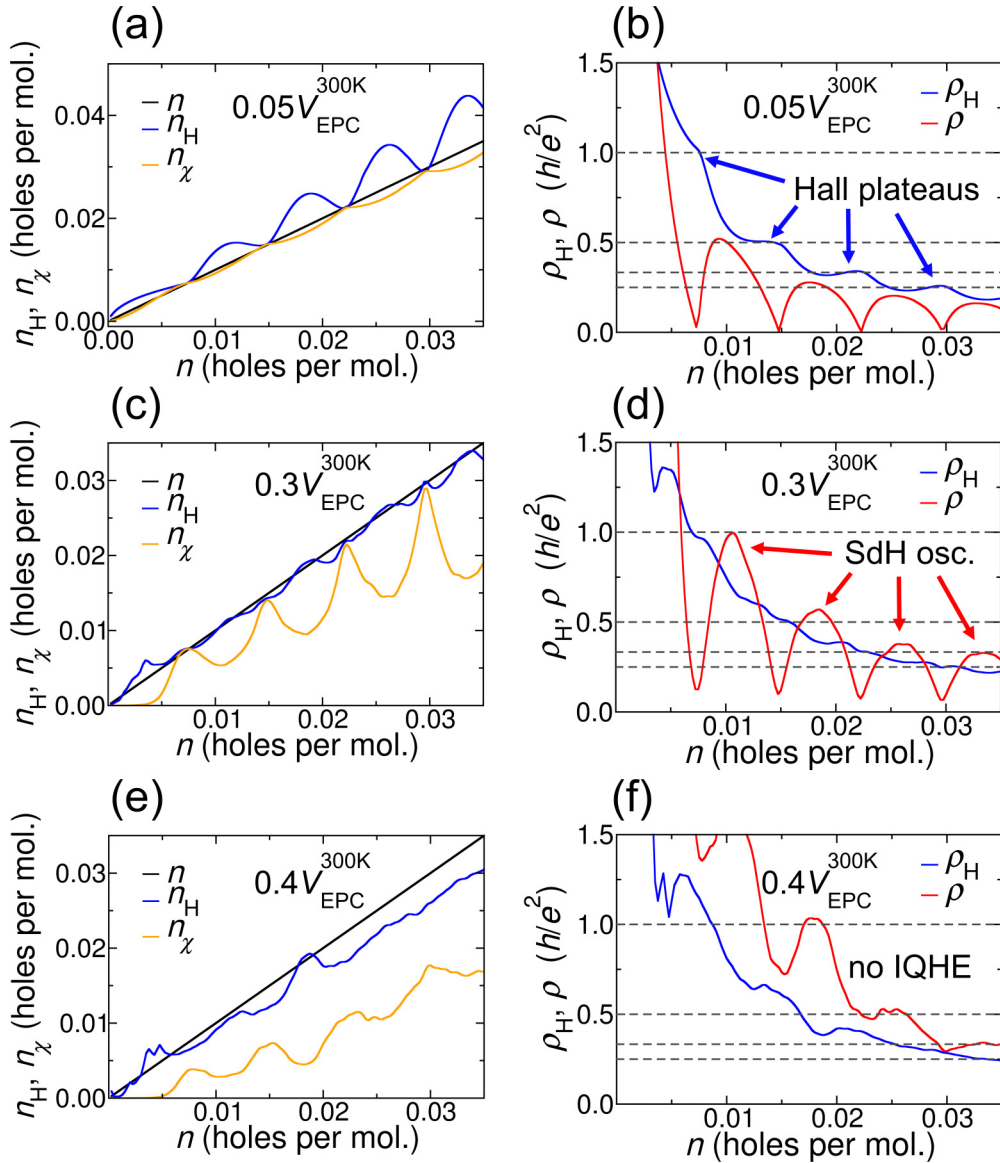


FIG. 5. IQHE in a rubrene monolayer at 60 T for reduced disorder strengths. (a),(c),(e) Hall density  $n_H$  and  $n_\chi$  as a function of the charge-carrier concentration for disorder strengths of 2.9 meV, 17.4 meV, and 23.0 meV. The carrier concentration  $n$  (solid black line) is also plotted for comparison. (b),(d),(f) Resistivity components  $\rho$  and  $\rho_H$  as a function of the total charge-carrier concentration for disorder strengths of 2.9 meV, 17.4 meV, and 23.0 meV. The dashed horizontal lines are the universal plateau heights of the IQHE regime.

vibrational disorder leads to a breakdown of this semiclassical orbital picture since  $n_\chi/n \approx 10^{-5}$  is much smaller.

Moreover, this behavior indicates the breakdown of any semiclassical transport picture as a consequence of multiple scattering at the vibrational disorder. Still, even in this regime, we find an ideal Hall effect ( $n = n_H$ ) at around room temperature and only moderate nonideality factors of about 0.5 when reducing temperature below 200 K. This ideal Hall effect in the transient localization regime is therefore distinguished from the semiclassical one in the intrinsic regime.

From these results we conclude that the presence of vibrational disorder (or disorder in general) has three significant effects. (i) The decay of  $\mu$  as well as  $n_H/n$  and  $n_\chi/n$  with the relaxation time  $\tau$ , indicating the presence of localized states, which do not spread after having reached their typical localization length. This reduces the absolute value of  $n_\chi$  yielding

a net value of orders of magnitudes smaller than in the pristine case. (ii) The difference between longitudinal and transverse response in the presence of disorder leads to nonidealities with  $n_H < n$ . (iii) Sufficiently large disorder can further lead to the intermixing, i.e., the hybridization of energetically separated holelike, electronlike, and open-orbit energy domains, which can also lead to a breakdown of the ideal Hall effect with a different characteristic.

Notwithstanding the detailed analysis of the present Hall-transport regime, no indication of possible quantization effects in the transport characteristics were found. Beyond the straightforward observation that the temperatures considered in Sec. III B are generally too high and magnetic fields possibly too low to observe quantization effects, there are primarily other reasons for their absence, prevailing even at sufficiently low  $T$  and high  $B_\gamma$ . Fortunately, the proposed theory facilitates

exploration of the transport regime, where the IQHE could emerge in organic semiconductors, and we wish to illustrate the conditions for the case of rubrene in the following section.

### C. IQHE in rubrene monolayers with disorder

We finally study the conditions for the emergence of the IQHE in rubrene monolayers with herringbone geometry in the presence of weak disorder. This scenario is suggested by transistor geometries where Hall transport occurs at the crystal surface in contact with the gate dielectric, leading to an ultrathin transport channel. For instance hexagonal boron nitride may be used as a dielectric layer to generate large-area crystal domains [10]. For the observation of the IQHE, a certain amount of disorder is needed to generate localized states near the edges of the Landau bands, leading to a vanishing channel resistance  $\rho$  and a quantized Hall resistance  $\rho_H$  of  $\rho_H = h/(e^2\nu)$  with  $\nu$  being an integer [17]. To model single herringbone planes of rubrene, we simply disregard the small electronic coupling perpendicular to the herringbone plane. Furthermore, we set the temperature to 0 K and increase  $B_y$  to 60 T to prepare suitable IQHE conditions, which can be realized in high-magnetic field labs [59]. Vibrational disorder is known to exist in rubrene at room temperature and we determine its value to  $V_{\text{EPC}}^{300\text{K}} = 57.5$  meV (cf. Appendix F). Taking this as a reference value, we study different strengths of reduced disorder (relative to  $V_{\text{EPC}}^{300\text{K}}$ ) in the following. Figure 5 compiles the calculated  $en_H$ ,  $en_\chi$ , and the resistivities  $\rho$  ( $\alpha$  direction) and  $\rho_H$ . We start in Figs. 5(a) and 5(b) discussing very small disorder strengths of 2.9 meV, which is below the spacing of the Landau-band centers ( $\approx 5$  meV). This value indeed leads to resistivity quantization in Fig. 5(b). Figure 5(a) shows that the Hall density  $n_H$  equals  $n_\chi$  at those carrier concentrations at which the Hall plateaus appear in  $\rho_H$ , while  $\rho$  vanishes in Fig. 5(b). The plateaus appear exactly with the quantized values of  $h/(e^2\nu)$ , which is the famous IQHE. The regions of vanishing channel resistance  $\rho$  are accompanied by pronounced SdH oscillations, indicating the presence of localized states.

The certainly stronger disorder in experiments can obscure this quantization of  $\rho_H$  under the chosen conditions for temperature and magnetic field. Therefore, assessing the stability of the IQHE against a stronger disorder is critical. When the disorder strength is increased to 30% of  $V_{\text{EPC}}^{300\text{K}}$  (17.4 meV), the previously distinct plateaus get smeared out [Fig. 5(d)], which coincides with the vanishing of the step structure of  $n_H$  plotted in Fig. 5(c). The density  $n_\chi$  only shows oscillations with varying carrier concentration indicating the pronounced intermixing of Landau bands due to the larger disorder. Despite the absence of clean Hall plateaus, we still observe clean SdH oscillations in  $\rho$  in Fig. 5(d). Further increasing the disorder to 40% of  $V_{\text{EPC}}^{300\text{K}}$  (23.0 meV) leads to a breakdown of the IQHE. Even the SdH oscillations, which are generally more resilient to stronger disorder, begin to diminish [see Fig. 5(f)]. Synchronously, the Hall density in Fig. 5(e) starts deviating from the charge-carrier density ( $n_H < n$ ), indicating that the Hall effect becomes nonideal. We explain this by the reduced localization length of transport states and the intermixing of Landau bands with different Chern numbers [60–62] caused by the increasing amount of disorder. The intermixing of the Landau bands is a consequence of the finite bandwidth of

the HOMO of rubrene leading to a complex superposition of different transport contributions. This reasoning for the transport regime of the IQHE is fully consistent with our interpretation of the Hall-transport regime for bulk crystals in Sec. III B. More explicitly, we conclude that the intermixing of Landau bands with different Chern numbers is similar to the intermixing of holelike, electronlike, and open-orbit energy domains as described above. We conclude that the intermixing of Landau bands and the intermixing of the three types of orbits is particularly important for OSCs since their typical electronic bandwidths remain usually below several hundreds of meV and *must* include both Landau bands with different Chern numbers as well as electronlike and holelike energy domains in the band structure in full agreement with the results for rubrene (cf. Figs. 1, 4, and 5).

## IV. SUMMARY AND CONCLUSION

In summary, this theoretical framework allows covering a variety of transport regimes, the concept of closed quasiparticle orbits in the BZ, temperature-dependent Hall transport in the presence of vibrational disorder, and topological quantum effects such as the IQHE. The regimes have been characterized by distinctive relationships between different densities and distinct mobility responses. The approach allows rationalizing in detail available experimental data and can be readily applied to the wide class of organic semiconducting materials. This will also support the interpretation of Hall measurements in the future and we hope to inspire further research in this direction.

## ACKNOWLEDGMENTS

We would like to thank the Deutsche Forschungsgemeinschaft for financial support [Projects No. OR-349/3 and No. OR-349/11 and the Clusters of Excellence e-conversion (Grant No. EXC2089) and MCQST (Grant No. EXC2111)]. Grants for computer time from the Leibniz Supercomputing Centre in Garching are gratefully acknowledged.

## APPENDIX A: DERIVATION OF THE dc CONDUCTIVITY

In this Appendix and in Appendix B, we derive Eq. (1) of the main text based on an efficient time-domain approach of the Kubo formalism [33]. For this purpose, we need to consider the general Kubo formula for the dc conductivity  $\sigma_{\alpha\beta}$  based on the linear response of the electric current density  $J_\alpha = \text{Tr}(\hat{\rho}\hat{j}_\alpha)$  to a constant electric field  $E_\beta$  [34],

$$\sigma_{\alpha\beta} = \frac{e^2}{V} \int_0^\infty dt f_{v_\alpha x_\beta}(t), \quad (\text{A1})$$

with the linear-response function  $f_{v_\alpha x_\beta}(t)$ . We may express  $f_{v_\alpha x_\beta}(t)$  in terms of spatial displacement operators  $\Delta\hat{x}_\alpha(t) = \hat{x}_\alpha(t) - \hat{x}_\alpha(0)$  as derived previously [33]:

$$f_{v_\alpha x_\beta}(t) = \frac{1}{2\hbar} \frac{d}{dt} \left[ \tan\left(\frac{\beta\hbar}{2} \frac{d}{dt}\right) \mathcal{D}_{x_\alpha x_\beta}^+(t) + \mathcal{D}_{x_\alpha x_\beta}^-(t) \right], \quad (\text{A2})$$

where the displacement-operator anticommutator function (DAF) is defined as

$$\mathcal{D}_{x_\alpha x_\beta}^\pm(t) = \text{Tr}(\hat{\rho}_0\{\Delta\hat{x}_\alpha(t), \Delta\hat{x}_\beta(t)\}) \quad (\text{A3})$$

and the displacement-operator commutator function (DCF) is defined as

$$\mathcal{D}_{x_\alpha x_\beta}^-(t) = -i \text{Tr}(\hat{\rho}_0[\Delta\hat{x}_\alpha(t), \Delta\hat{x}_\beta(t)]). \quad (\text{A4})$$

The square brackets and the curly brackets denote the commutator and the anticommutator of the spatial displacements, respectively. The time evolution of the involved operators is governed by the Hamiltonian  $\hat{H}$ , while for the thermal average the grand-canonical equilibrium density operator  $\hat{\rho}_0 = e^{-\beta(\hat{H}-\mu\hat{N})}/\text{Tr}(e^{-\beta(\hat{H}-\mu\hat{N})})$  is used. We note that the initial values of the DAF and the DCF vanish, i.e.,  $\mathcal{D}_{x_\alpha x_\beta}^\pm(0) = 0$ .

As a first step of the derivation of Eq. (1), we prove that Eqs. (A1) to (A4) can be written as

$$\sigma_{\alpha\beta} = \frac{e^2}{2V} \lim_{t \rightarrow \infty} \left[ \frac{\beta}{2} \frac{d}{dt} \mathcal{D}_{x_\alpha x_\beta}^+(t) + \frac{1}{\hbar} \mathcal{D}_{x_\alpha x_\beta}^-(t) \right]. \quad (\text{A5})$$

Towards this end, the second term in Eq. (A5) is readily obtained via time integration,

$$\frac{e^2}{2\hbar V} \int_0^\infty dt \frac{d}{dt} \mathcal{D}_{x_\alpha x_\beta}^-(t) = \frac{e^2}{2\hbar V} \lim_{t \rightarrow \infty} \mathcal{D}_{x_\alpha x_\beta}^-(t). \quad (\text{A6})$$

The first term of Eq. (1) is derived from the first term in Eq. (A2) and requires more steps. It can be identified with the time-symmetric part of the linear response function

$$f_{v_\alpha v_\beta}^{\text{ts}}(t) = \frac{1}{2\hbar} \tan\left(\frac{\beta\hbar}{2} \frac{d}{dt}\right) \frac{d}{dt} \mathcal{D}_{x_\alpha x_\beta}^+(t). \quad (\text{A7})$$

Next, we use that the second derivative of the DAF with respect to  $t$  can be expressed with the time-symmetric part of the current-current correlation function

$$\mathcal{S}_{v_\alpha v_\beta}(t) = \frac{1}{2} \text{Tr}(\hat{\rho}_0\{\hat{v}_\beta(0), \hat{v}_\alpha(t)\}) \quad (\text{A8})$$

according to

$$\mathcal{S}_{v_\alpha v_\beta}^{\text{ts}}(t) = \frac{1}{4} \frac{d^2}{dt^2} \mathcal{D}_{x_\alpha x_\beta}^+(t). \quad (\text{A9})$$

Its substitution into Eq. (A7) yields

$$f_{v_\alpha v_\beta}^{\text{ts}}(t) = \beta \frac{\tan\left(\frac{\beta\hbar}{2} \frac{d}{dt}\right)}{\frac{\beta\hbar}{2} \frac{d}{dt}} \mathcal{S}_{v_\alpha v_\beta}^{\text{ts}}(t). \quad (\text{A10})$$

As a next step, we express  $\mathcal{S}_{v_\alpha v_\beta}^{\text{ts}}(t)$  by its Fourier transform and obtain

$$f_{v_\alpha v_\beta}^{\text{ts}}(t) = \beta \frac{\tan\left(\frac{\beta\hbar}{2} \frac{d}{dt}\right)}{\frac{\beta\hbar}{2} \frac{d}{dt}} \left( \frac{1}{2\pi} \int_{-\infty}^\infty d\omega e^{i\omega t} \mathcal{S}_{v_\alpha v_\beta}^{\text{ts}}(\omega) \right), \quad (\text{A11})$$

which can be simplified by applying the differential operator onto the exponential function, yielding

$$f_{v_\alpha v_\beta}^{\text{ts}}(t) = \frac{\beta}{2\pi} \int_{-\infty}^\infty d\omega e^{i\omega t} \frac{\tanh\left(\frac{\beta\hbar\omega}{2}\right)}{\frac{\beta\hbar\omega}{2}} \mathcal{S}_{v_\alpha v_\beta}^{\text{ts}}(\omega). \quad (\text{A12})$$

Calculating the time integral results in

$$\begin{aligned} \int_0^\infty dt f_{v_\alpha v_\beta}^{\text{ts}}(t) &= \frac{\beta}{2\pi} \int_{-\infty}^\infty d\omega \left( \pi \delta(\omega) + \frac{i}{\omega} \right) \\ &\quad \times \frac{\tanh\left(\frac{\beta\hbar\omega}{2}\right)}{\frac{\beta\hbar\omega}{2}} \mathcal{S}_{v_\alpha v_\beta}^{\text{ts}}(\omega). \end{aligned} \quad (\text{A13})$$

Since the function  $\mathcal{S}_{v_\alpha v_\beta}^{\text{ts}}(t)$  is real and time symmetric, its Fourier transform  $\mathcal{S}_{v_\alpha v_\beta}^{\text{ts}}(\omega)$  is  $\omega$  symmetric. Due to this symmetry, the second term on the right-hand side of Eq. (A13) vanishes because an odd function is integrated over a symmetric interval. Consequently, we remain with the first term given by

$$\begin{aligned} \int_0^\infty dt f_{v_\alpha v_\beta}^{\text{ts}}(t) &= \frac{\beta}{2} \mathcal{S}_{v_\alpha v_\beta}^{\text{ts}}(\omega = 0) \\ &= \beta \int_0^\infty dt \mathcal{S}_{v_\alpha v_\beta}^{\text{ts}}(t) \\ &= \frac{\beta}{4} \int_0^\infty dt \frac{d^2}{dt^2} \mathcal{D}_{x_\alpha x_\beta}^+(t). \end{aligned} \quad (\text{A14})$$

This identity can be integrated over time yielding the desired form of the first term of Eq. (A5):

$$\frac{\beta}{4} \int_0^\infty dt \frac{d^2}{dt^2} \mathcal{D}_{x_\alpha x_\beta}^+(t) = \frac{\beta}{4} \lim_{t \rightarrow \infty} \frac{d}{dt} \mathcal{D}_{x_\alpha x_\beta}^+(t), \quad (\text{A15})$$

because also the time derivative of  $\mathcal{D}_{x_\alpha x_\beta}^+(t)$  vanishes at zero time. We thus have shown that the dc limit of the electrical conductivity is given by Eq. (A5) in its general form.

We proceed by introducing a finite relaxation time  $\tau$  and rewrite Eq. (A5) as

$$\sigma_{\alpha\beta} = \lim_{\tau \rightarrow \infty} \sigma_{\alpha\beta}(\tau), \quad (\text{A16})$$

with

$$\sigma_{\alpha\beta}(\tau) = \frac{e^2}{2V} \int_0^\infty dt e^{-\frac{t}{\tau}} \left[ \frac{\beta}{2} \frac{d^2}{dt^2} \mathcal{D}_{x_\alpha x_\beta}^+(t) + \frac{1}{\hbar} \frac{d}{dt} \mathcal{D}_{x_\alpha x_\beta}^-(t) \right], \quad (\text{A17})$$

which we evaluate explicitly for noninteracting quasiparticles in Appendix B to obtain Eq. (1).

## APPENDIX B: DERIVATION OF THE dc CONDUCTIVITY FOR INDEPENDENT QUASIPARTICLES

To obtain Eq. (1) of the main text, we assume quasi-noninteracting (fermionic) quasiparticles, which applies if the Hamiltonian of the system has the common form

$$\hat{H} = \sum_k \varepsilon_k \hat{c}_k^\dagger \hat{c}_k, \quad (\text{B1})$$

with the eigenenergies  $\varepsilon_k$  and the fermionic creation and annihilation operators  $\hat{c}_k^\dagger$  and  $\hat{c}_k$ . Based on this assumption, we can further simplify the many-body thermal averages in the DAF and the DCF by applying Wick's theorem [63]. In general, we can write the electric dipole operator in terms of the fermionic eigenmodes as

$$e\hat{x}_\alpha = e \sum_{kl} x_{kl}^\alpha \hat{c}_k^\dagger \hat{c}_l. \quad (\text{B2})$$

The corresponding displacement operator is then simply evaluated as

$$\Delta\hat{x}_\alpha(t) = \sum_{kl} (e^{\frac{i\hbar}{\tau}(\varepsilon_k - \varepsilon_l)} - 1) x_{kl}^\alpha \hat{c}_k^\dagger \hat{c}_l = \sum_{kl} \Delta x_{kl}^\alpha(t) \hat{c}_k^\dagger \hat{c}_l. \quad (\text{B3})$$

For the DAF, we thus find

$$\mathcal{D}_{x_\alpha x_\beta}^+(t) = \int_{-\infty}^{\infty} dE \int_{-\infty}^{\infty} dE' f(E') [1 - f(E)] \text{Tr}[\delta(E - \hat{H}) \Delta \hat{x}_\alpha(t) \delta(E' - \hat{H}) \Delta \hat{x}_\beta(t) + \text{H.c.}], \quad (\text{B4})$$

where we have introduced the spectral projection operator  $\delta(E - \hat{H})$  and the completeness relation  $\mathbb{1} = \int_{-\infty}^{\infty} dE \delta(E - \hat{H})$  with respect to the one-particle spectrum of the Hamiltonian. For the second derivative of the DAF, we obtain

$$\begin{aligned} \frac{d^2}{dt^2} \mathcal{D}_{x_\alpha x_\beta}^+(t) &= 2 \int_{-\infty}^{\infty} dE \int_{-\infty}^{\infty} dE' f(E') [1 - f(E)] \cos\left(\frac{t(E - E')}{\hbar}\right) \\ &\times \text{Tr}[\delta(E - \hat{H}) \hat{v}_\alpha(0) \delta(E' - \hat{H}) \hat{v}_\beta(0) + \text{H.c.}]. \end{aligned} \quad (\text{B5})$$

From this relation, we find

$$\begin{aligned} \int_0^\infty dt e^{-\frac{t}{\tau}} \frac{d^2}{dt^2} \mathcal{D}_{x_\alpha x_\beta}^+(t) &= 2\hbar\pi \int_{-\infty}^{\infty} dE \int_{-\infty}^{\infty} dE' f(E') [1 - f(E)] \frac{1}{\pi} \frac{\frac{\hbar}{\tau}}{\frac{\hbar^2}{\tau^2} + (E - E')^2} \\ &\times \text{Tr}[\delta(E - \hat{H}) \hat{v}_\alpha(0) \delta(E' - \hat{H}) \hat{v}_\beta(0) + \text{H.c.}]. \end{aligned} \quad (\text{B6})$$

In this expression, we see that the energy integrals include a convolution with the Dirac series  $\delta_\tau(E - E') = \hbar/(\pi\tau)/[\hbar^2/\tau^2 + (E - E')^2]$ , which corresponds to a match in the one-particle energies  $E = E'$  in the limit  $\tau \rightarrow \infty$ . For the one-particle DAF, which is introduced in Eq. (2), we obtain

$$\int_0^\infty dt e^{-\frac{t}{\tau}} \frac{d^2}{dt^2} \mathcal{D}_{x_\alpha x_\beta}^+(E, t) = 2\pi\hbar \int_{-\infty}^{\infty} dE' \delta_\tau(E - E') \text{Tr}[\delta(E - \hat{H}) \hat{v}_\alpha(0) \delta(E' - \hat{H}) \hat{v}_\beta(0) + \text{H.c.}]. \quad (\text{B7})$$

Therefore, using Eqs. (B6) and (B7), we find

$$\begin{aligned} \beta \int_0^\infty dt e^{-\frac{t}{\tau}} \frac{d^2}{dt^2} \mathcal{D}_{x_\alpha x_\beta}^+(t) &= - \int_0^\infty dt e^{-\frac{t}{\tau}} \int_{-\infty}^{\infty} dE \frac{df(E)}{dE} \frac{d^2}{dt^2} \mathcal{D}_{x_\alpha x_\beta}^+(E, t) \\ &+ \int_0^\infty dt \int_{-\infty}^{\infty} dE \int_{-\infty}^{\infty} dE' O(\delta_\tau(E - E')) [f(E) - f(E')]. \end{aligned} \quad (\text{B8})$$

The above relation includes the expression used for the calculation of the symmetric part of the electrical conductivity tensor in Eq. (1). The residual term in Eq. (B8) vanishes for degenerate states, i.e., for  $E = E'$  and for  $\hbar/\tau \ll E - E'$ , i.e., if external relaxation mechanisms are considered small against the energy differences (as usually considered). Thus we approximate the full DAF with the one-particle DAF as

$$\beta \int_0^\infty dt e^{-\frac{t}{\tau}} \frac{d^2}{dt^2} \mathcal{D}_{x_\alpha x_\beta}^+(t) \approx - \int_0^\infty dt e^{-\frac{t}{\tau}} \int_{-\infty}^{\infty} dE \frac{df(E)}{dE} \frac{d^2}{dt^2} \mathcal{D}_{x_\alpha x_\beta}^+(E, t) \quad (\text{B9})$$

for any given relaxation time  $\tau$ . In the limit  $\tau \rightarrow \infty$ , we find the identity

$$\beta \lim_{t \rightarrow \infty} \frac{d}{dt} \mathcal{D}_{x_\alpha x_\beta}^+(t) = - \lim_{\tau \rightarrow \infty} \int_0^\infty dt e^{-\frac{t}{\tau}} \int_{-\infty}^{\infty} dE \frac{df(E)}{dE} \frac{d^2}{dt^2} \mathcal{D}_{x_\alpha x_\beta}^+(E, t) = - \int_{-\infty}^{\infty} dE \frac{df(E)}{dE} \lim_{t \rightarrow \infty} \frac{d}{dt} \mathcal{D}_{x_\alpha x_\beta}^+(E, t). \quad (\text{B10})$$

The DCF can be evaluated equivalently to Eq. (B5):

$$\mathcal{D}_{x_\alpha x_\beta}^-(t) = \int_{-\infty}^{\infty} dE f(E) \mathcal{D}_{x_\alpha x_\beta}^-(E, t), \quad (\text{B11})$$

where  $\mathcal{D}_{x_\alpha x_\beta}^-(E, t)$  is the one-particle DCF given in Eq. (3). Collecting the two expressions in Eqs. (B10) and (B11) yields

$$\sigma_{\alpha\beta} = \lim_{\tau \rightarrow \infty} \sigma_{\alpha\beta}(\tau), \quad (\text{B12})$$

with

$$\sigma_{\alpha\beta}(\tau) = \frac{e^2}{2V} \int_0^\infty dt e^{-\frac{t}{\tau}} \int_{-\infty}^{\infty} dE \left[ -\frac{1}{2} \frac{df(E)}{dE} \frac{d^2}{dt^2} \mathcal{D}_{x_\alpha x_\beta}^+(E, t) + \frac{1}{\hbar} f(E) \frac{d}{dt} \mathcal{D}_{x_\alpha x_\beta}^-(E, t) \right], \quad (\text{B13})$$

which is Eq. (1).

### APPENDIX C: INTRINSIC HALL CONDUCTIVITY AND ORBITING PICTURE

In this section, we evaluate the intrinsic Hall conductivity in the absence of disorder and connect it to semiclassical expressions from semiclassical band theory. As a first step, we write the quasiparticle Hamiltonian without external potential but coupled to the operator for the vector potential  $\hat{\mathbf{A}}$ ,

$$\hat{H} = \hat{H}(\hat{\mathbf{p}} - q\hat{\mathbf{A}}). \quad (\text{C1})$$

Here, we consider a homogeneous magnetic field  $\mathbf{B} = \nabla \times \mathbf{A}$ , which we may realize using the symmetric gauge for the operator of the vector potential  $\hat{\mathbf{A}} = \frac{1}{2}\mathbf{B} \times \hat{\mathbf{x}}$ . We now set the magnetic field to  $\mathbf{B} = B_\gamma \mathbf{e}_\gamma$ , where  $\mathbf{e}_\gamma$  is perpendicular to the transport directions  $\mathbf{e}_\alpha$  and  $\mathbf{e}_\beta$  yielding the vector potential  $\hat{\mathbf{A}} = (-B_\gamma \hat{x}_\beta/2, B_\gamma \hat{x}_\alpha/2, 0)$ . We now introduce the kinetic momenta  $\hat{\pi}_\alpha^\pm = \hat{p}_\alpha \pm q\hat{A}_\alpha$  and  $\hat{\pi}_\beta^\pm = \hat{p}_\beta \pm q\hat{A}_\beta$ . This transformation can be used to express both the position and canonical momentum operators with  $\hat{\pi}_{\alpha/\beta}^\pm$  according to

$$\begin{aligned} \hat{x}_\alpha &= \frac{1}{qB_\gamma}(\hat{\pi}_\beta^+ - \hat{\pi}_\beta^-), & \hat{p}_\alpha &= \frac{1}{2}(\hat{\pi}_\beta^+ + \hat{\pi}_\beta^-), \\ \hat{x}_\beta &= \frac{1}{qB_\gamma}(\hat{\pi}_\alpha^- - \hat{\pi}_\alpha^+), & \hat{p}_\beta &= \frac{1}{2}(\hat{\pi}_\alpha^+ + \hat{\pi}_\alpha^-). \end{aligned} \quad (\text{C2})$$

This turns out to be convenient since the Hamiltonian then solely depends on the kinetic momenta  $\hat{\pi}_\alpha^-$  and  $\hat{\pi}_\beta^-$ . The kinetic momentum operators satisfy the commutation relations

$$\begin{aligned} [\hat{\pi}_\alpha^-, \hat{\pi}_\beta^-] &= [\hat{\pi}_\beta^+, \hat{\pi}_\alpha^+] = i\hbar q B_\gamma, \\ [\hat{\pi}_\alpha^-, \hat{\pi}_\alpha^+] &= [\hat{\pi}_\beta^-, \hat{\pi}_\beta^+] = [\hat{\pi}_\alpha^-, \hat{\pi}_\beta^+] = [\hat{\pi}_\beta^-, \hat{\pi}_\alpha^+] = 0. \end{aligned} \quad (\text{C3})$$

We now evaluate the Heisenberg equation of motion for the kinetic momentum operators:

$$\begin{aligned} \dot{\hat{\pi}}_\alpha^+(t) &= 0, & \dot{\hat{\pi}}_\alpha^-(t) &= qB_\gamma \frac{\partial \hat{H}}{\partial \hat{\pi}_\beta^-}(t), \\ \dot{\hat{\pi}}_\beta^+(t) &= 0, & \dot{\hat{\pi}}_\beta^-(t) &= -qB_\gamma \frac{\partial \hat{H}}{\partial \hat{\pi}_\alpha^-}(t), \end{aligned} \quad (\text{C4})$$

and find a simple relation between the time derivatives of the position and the kinetic momentum operators

$$\dot{\hat{x}}_\alpha^-(t) = qB_\gamma \hat{v}_\beta(t), \quad (\text{C5})$$

$$\dot{\hat{x}}_\beta^-(t) = -qB_\gamma \hat{v}_\alpha(t). \quad (\text{C6})$$

To evaluate the Hall conductivity  $\sigma_H$  for this case, we decompose it into two terms

$$\sigma_H = \sigma_H^I + \sigma_H^{II}, \quad (\text{C7})$$

with

$$\begin{aligned} \sigma_H^I &= \frac{e^2}{2V} \int_{-\infty}^{\infty} dE f(E) \text{Tr}[\delta(E - \hat{H})(\hat{v}_\alpha [\text{Re}\hat{G}(E), \hat{x}_\beta] \\ &\quad - \hat{v}_\beta [\text{Re}\hat{G}(E), \hat{x}_\alpha])], \end{aligned} \quad (\text{C8})$$

$$\sigma_H^{II} = \frac{e^2}{2V} \int_{-\infty}^{\infty} dE f(E) \text{Tr}\left[\frac{d}{dE} \delta(E - \hat{H})(\hat{x}_\alpha \hat{v}_\beta - \hat{x}_\beta \hat{v}_\alpha)\right], \quad (\text{C9})$$

where  $\text{Re}\hat{G}(E) = (E - \hat{H})^{-1}$  is the real part of the Green's function. This decomposition of  $\sigma_H$  is derived in detail in Appendixes D and E. We first calculate the second term of the Hall conductivity  $\sigma_H^{II}$  by using the equations of motion for the kinetic momenta,

$$\begin{aligned} \text{Tr}[\delta(E - \hat{H})(\hat{v}_\alpha \hat{x}_\beta - \hat{v}_\beta \hat{x}_\alpha)] \\ = \frac{1}{e^2 B_\gamma^2} \text{Tr}[\delta(E - \hat{H})(\dot{\hat{\pi}}_\alpha^- \hat{\pi}_\beta^- - \dot{\hat{\pi}}_\beta^- \hat{\pi}_\alpha^-)], \end{aligned} \quad (\text{C10})$$

where we have used that the operators  $\hat{\pi}_\alpha^+$  and  $\hat{\pi}_\beta^+$  commute with the Hamiltonian. We note that the expectation value only depends on the conjugate operators  $\hat{\pi}_\alpha^-$  and  $\hat{\pi}_\beta^-$ .

To obtain the semiclassical result for the Hall conductivity, we now substitute the quantum mechanical trace with the integral over the phase space

$$\begin{aligned} \text{Tr}[\delta(E - \hat{H})(\dots)] \rightarrow \frac{1}{(2\pi\hbar)^2} \int dx_\alpha dx_\beta dp_\alpha dp_\beta \\ \times \delta(E - \varepsilon(\pi_\alpha^-, \pi_\beta^-))(\dots), \end{aligned} \quad (\text{C11})$$

which we can substitute with the integral over the kinetic momenta using the coordinate transformation in Eq. (C2):

$$\begin{aligned} \frac{1}{(2\pi\hbar)^2} \int dx_\alpha dx_\beta dp_\alpha dp_\beta \delta(E - \varepsilon(\pi_\alpha^-, \pi_\beta^-))(\dots) \\ = \frac{1}{(2\pi\hbar e B_\gamma)^2} \int d\pi_\alpha^+ d\pi_\beta^+ d\pi_\alpha^- d\pi_\beta^- \\ \times \delta(E - \varepsilon(\pi_\alpha^-, \pi_\beta^-))(\dots). \end{aligned} \quad (\text{C12})$$

Since the total number of states is given by

$$\begin{aligned} N &= \int_{-\infty}^{\infty} dE \text{Tr}(\delta(E - \hat{H})) \\ &\rightarrow \frac{1}{(2\pi\hbar e B_\gamma)^2} \int d\pi_\alpha^+ d\pi_\beta^+ d\pi_\alpha^- d\pi_\beta^-, \end{aligned} \quad (\text{C13})$$

we obtain its semiclassical result as

$$N = \frac{\Omega^2}{(2\pi\hbar e B_\gamma)^2}, \quad (\text{C14})$$

with  $\Omega$  being the phase-space volume of the kinetic momenta:

$$\Omega = \int d\pi_\alpha^+ d\pi_\beta^+ = \int d\pi_\alpha^- d\pi_\beta^-. \quad (\text{C15})$$

The expectation value entering the Hall conductivity then reads

$$\begin{aligned} \text{Tr}[\delta(E - \hat{H})(\dot{\hat{\pi}}_\alpha^- \hat{\pi}_\beta^- - \dot{\hat{\pi}}_\beta^- \hat{\pi}_\alpha^-)] \\ = \frac{N}{\Omega} \int d\pi_\alpha^- d\pi_\beta^- \delta(E - \varepsilon(\pi_\alpha^-, \pi_\beta^-))(\dot{\pi}_\alpha^- \pi_\beta^- - \dot{\pi}_\beta^- \pi_\alpha^-), \end{aligned} \quad (\text{C16})$$

where the integration over the kinetic momenta  $\pi_\alpha^+$  and  $\pi_\beta^+$  amounts to the phase-space volume  $\Omega$  since the integrand is independent of these coordinates for the present model. We now may substitute the integral over the phase space of kinetic momenta with the integral along all quasiparticle orbits of constant energy (which represents the Fermi surface in the

case of a 2D system):

$$\begin{aligned} & \frac{N}{\Omega} \int d\pi_{\alpha}^{-} d\pi_{\beta}^{-} \delta(E - \varepsilon(\pi_{\alpha}^{-}, \pi_{\beta}^{-})) (\dot{\pi}_{\alpha}^{-} \pi_{\beta}^{-} - \dot{\pi}_{\beta}^{-} \pi_{\alpha}^{-}) \\ &= \frac{N}{\Omega} \int_{\text{orbits}} d\pi \frac{1}{|\nabla_{\pi} \varepsilon(\pi_{\alpha}^{-}, \pi_{\beta}^{-})|} (\dot{\pi}_{\alpha}^{-} \pi_{\beta}^{-} - \dot{\pi}_{\beta}^{-} \pi_{\alpha}^{-}). \end{aligned} \quad (\text{C17})$$

Using the equations of motion to substitute  $|\nabla_{\pi} \varepsilon(\pi_{\alpha}^{-}, \pi_{\beta}^{-})| = |\dot{\pi}|/eB_{\gamma}$ , we obtain

$$\begin{aligned} & \frac{N}{\Omega} \int_{\text{orbits}} d\pi \frac{1}{|\nabla_{\pi} \varepsilon(\pi_{\alpha}^{-}, \pi_{\beta}^{-})|} (\dot{\pi}_{\alpha}^{-} \pi_{\beta}^{-} - \dot{\pi}_{\beta}^{-} \pi_{\alpha}^{-}) \\ &= \frac{N}{\Omega} \int_{\text{orbits}} d\pi \frac{eB_{\gamma}}{|\dot{\pi}|} [\dot{\pi}_{\alpha}^{-} \pi_{\beta}^{-} - \dot{\pi}_{\beta}^{-} \pi_{\alpha}^{-}] \\ &= \frac{NeB_{\gamma}}{\Omega} \left( \int_{\text{orbits}} d\pi \times \pi \right)_{\gamma}. \end{aligned} \quad (\text{C18})$$

The  $\gamma$  component of the integral  $\int_{\text{orbits}} d\pi \times \pi$  is related to the area  $A_e(E) - A_h(E)$  enclosed by all semiclassical orbits with energy  $E$  via

$$\left( \int_{\text{orbits}} d\pi \times \pi \right)_{\gamma} = 2[A_e(E) - A_h(E)] \quad (\text{C19})$$

leading to

$$\text{Tr}[\delta(E - \hat{H})(\dot{\pi}_{\alpha}^{-} \pi_{\beta}^{-} - \dot{\pi}_{\beta}^{-} \pi_{\alpha}^{-})] = 2NeB_{\gamma} \frac{A_e(E) - A_h(E)}{\Omega}. \quad (\text{C20})$$

We now see that the expectation value is proportional to the difference of the areas  $A_e(E) - A_h(E)$  covered by electronlike and holelike states in the phase space, which are enclosed by all quasiparticle orbits with energy  $E$ . Thus we obtain the Hall conductivity  $\sigma_{\text{H}}^{\text{II}}$  as

$$\sigma_{\text{H}}^{\text{II}} = \frac{eN}{B_{\gamma}V} \int_{-\infty}^{\infty} dE f(E) \frac{d}{dE} \frac{A_e(E) - A_h(E)}{\Omega}. \quad (\text{C21})$$

In the same way, the remaining term  $\sigma_{\text{H}}^{\text{I}}$  can be obtained using

$$\begin{aligned} & \text{Tr}[\delta(E - \hat{H})([\hat{x}_{\beta}, \hat{v}_{\alpha} \text{Re}\hat{G}(E)] - [\hat{x}_{\alpha}, \hat{v}_{\beta} \text{Re}\hat{G}(E)])] \\ &= \frac{1}{e^2 B_{\gamma}^2} \text{Tr}[\delta(E - \hat{H})(\dot{\pi}_{\alpha}^{-} [\hat{\pi}_{\beta}^{-}, \text{Re}\hat{G}(E)] + \text{H.c.})]. \end{aligned} \quad (\text{C22})$$

The semiclassical result of this expectation value is obtained by substituting the commutator under the trace with the Poisson bracket:

$$[\dots, \dots] \rightarrow i\hbar q B_{\gamma} \{\dots, \dots\}. \quad (\text{C23})$$

We find

$$\begin{aligned} & \frac{1}{e^2 B_{\gamma}^2} \text{Tr}[\delta(E - \hat{H})(\dot{\pi}_{\alpha}^{-} [\hat{\pi}_{\beta}^{-}, \text{Re}\hat{G}(E)] + \text{H.c.})] \\ &= -\frac{iq\hbar N}{e\Omega} \int_{\text{orbits}} d\pi \cdot \nabla_{\pi} \text{Re}G(E) \\ &= 0, \end{aligned} \quad (\text{C24})$$

because the real part of the Green's function at energy  $E$  is constant along all quasiparticle orbits. Therefore, we obtain

$$\sigma_{\text{H}}^{\text{I}} = 0, \quad (\text{C25})$$

which means that  $\sigma_{\text{H}}^{\text{I}}$  vanishes identically in the semiclassical limit. We thus obtain for the total intrinsic Hall conductivity as given in Eq. (21)

$$\sigma_{\text{H}}^{\text{sc}} = \sigma_{\text{H}}^{\text{II}} = \frac{eN}{B_{\gamma}V} \int_{-\infty}^{\infty} dE f(E) \frac{d}{dE} \frac{A_e(E) - A_h(E)}{\Omega_{\text{BZ}}}, \quad (\text{C26})$$

where we have substituted the phase-space volume  $\Omega$  with the volume of the Brillouin zone in the reciprocal space via  $\Omega = \hbar^2 \Omega_{\text{BZ}}$  and redefined  $A_e(E) - A_h(E)$  with the area enclosed by the quasiparticle orbits in the reciprocal space. Based on the numerical results for the Hall conductivity, we may approximate the Hall conductivity solely in terms of the specific distribution of closed and open orbits associated with electron- and holelike behavior. We have found the following intuitive expression for the Hall conductivity (at zero temperature):

$$\sigma_{\text{H}}(E_{\text{F}}) \approx -\frac{e}{B_{\gamma}} \{n_e \Theta(E_{\text{F}} - E_e) - (1 - n_e)[1 - \Theta(E_{\text{F}} - E_h)]\}, \quad (\text{C27})$$

which agrees with Eq. (22) if we set the carrier density of the holes to  $n = n_h = 1 - n_e$ . The energies  $E_e$  and  $E_h$  correspond to the critical energies, up to which closed electronlike and holelike orbits appear at the Fermi energy  $E_{\text{F}}$ .

We now connect these general findings to the results for the intrinsic Hall conductivity of rubrene in Figs. 1(b) and 1(d). The energy dependence of  $\sigma_{\text{H}}$  in Fig. 1(b) [or Fig. 1(c) for  $en_{\chi}$ ] can be explained if we consider only the holelike orbits with a Fermi energy larger than 103 meV (and for zero temperature). In this case, all quasiparticle orbits are closed and the area difference  $A_e(E_{\text{F}}) - A_h(E_{\text{F}})$  is equal to the area covered by the occupied hole states in the BZ  $A_{\text{occ}}(E_{\text{F}})$ , which is related to the carrier concentration  $n = N_{\text{occ}}(E_{\text{F}})/V$  by  $n/N = A_{\text{occ}}(E_{\text{F}})/\Omega_{\text{BZ}}$  with the number of occupied states  $N_{\text{occ}}(E_{\text{F}})$ . Then, from Eq. (C26) we immediately get  $\sigma_{\text{H}} = qN/(B_{\gamma}V)A_{\text{occ}}(E_{\text{F}})/\Omega_{\text{BZ}} = en/B_{\gamma}$ . This ideal behavior is perfectly satisfied in Figs. 1(b) and 1(c) for Fermi energies above 103 meV, i.e., the holelike states. If the Fermi energy lies between these values, the orbits are open in the BZ and the Hall conductivity becomes zero in qualitative agreement with the numerical result of Figs. 1(b) and 1(c). Then for Fermi energies below  $-202$  meV a very small domain of electronlike orbits manifesting as a small negative peak in Figs. 1(b) and 1(c) is observed in full agreement with the pristine band structure of rubrene.

We note that Eq. (C27) [i.e., Eq. (22)] is only an approximate realization of Eq. (C26) [i.e., Eq. (21)] and may further depend on the details of the band structure in, e.g., three-dimensional bulk systems and if more complex band structures are considered, which may include multiple electronlike, holelike, and open-orbit domains.

#### APPENDIX D: EQUILIBRIUM VALUE OF dc-CONDUCTIVITY TENSOR

To prove the semiclassical expression for the Hall conductivity in Eq. (21) of the main text, we need to determine the equilibrium value of the dc conductivity based on Eq. (1) for  $\tau \rightarrow \infty$ . After this derivation and in Appendix E, we connect the present time-domain approach with known forms of the

dc conductivity derived within the Kubo formalism such as the Kubo-Bastin formula [43] and the Berry curvature that enters the TKNN formula [20,36]. Hence we evaluate the time integral in the symmetric part of the conductivity tensor  $\sigma_{\alpha\beta}^s$  in Eq. (4). In the energy eigenbasis, we find for  $\sigma_{\alpha\beta}^s$

$$\sigma_{\alpha\beta}^s = \frac{\beta e^2 \pi \hbar}{2V} \sum_{mn} f(\varepsilon_n) [1 - f(\varepsilon_m)] \delta(\varepsilon_n - \varepsilon_m) \times (v_{nm}^\alpha v_{mn}^\beta + v_{nm}^\beta v_{mn}^\alpha), \quad (\text{D1})$$

where we write the matrix elements  $v_{mn}^\alpha = v_{mn}^\alpha(0)$  as a short-hand notation. This expression is the equilibrium value for the symmetric part of the conductivity and generalizes the Kubo-Greenwood formula for longitudinal charge transport [41,42], which can be seen by using the completeness relation  $\mathbb{1} = \int_{-\infty}^{\infty} dE \delta(E - \hat{H})$ :

$$\sigma_{\alpha\beta}^s = \frac{\beta e^2 \pi \hbar}{V} \int_{-\infty}^{\infty} dE f(E) [1 - f(E)] \times \text{Tr}[\delta(E - \hat{H}) \hat{v}_\alpha \delta(E - \hat{H}) \hat{v}_\beta]. \quad (\text{D2})$$

The evaluation of the time integral in the Hall conductivity for independent particles [see Eq. (5)] results in the following expression:

$$\sigma_H = -\frac{e^2}{V} \sum_{mn} \frac{f(\varepsilon_n)}{\varepsilon_n - \varepsilon_m} (v_{nm}^\alpha x_{mn}^\beta - v_{nm}^\beta x_{mn}^\alpha), \quad (\text{D3})$$

where we have used the matrix elements of the velocity operator  $v_{nm}^\alpha = i(\varepsilon_n - \varepsilon_m) x_{nm}^\alpha / \hbar$ . Furthermore, we may alternatively derive the Hall conductivity by using the following identity:

$$\begin{aligned} \frac{d^2}{dt^2} \mathcal{D}_{x_\alpha x_\beta}^-(t) &= -2\hbar f_{v_\alpha v_\beta}(0) - \mathcal{D}_{v_\alpha v_\beta}^-(t) \\ &= -2i \sum_{mn} f(\varepsilon_n) (v_{nm}^\alpha v_{mn}^\beta - v_{nm}^\beta v_{mn}^\alpha) \\ &\quad \times \cos\left(\frac{t(\varepsilon_n - \varepsilon_m)}{\hbar}\right), \end{aligned} \quad (\text{D4})$$

where  $f_{v_\alpha v_\beta}(0)$  is the linear response function of the velocity operators at zero time [33]. We then find for the Hall conductivity

$$\sigma_H = \frac{i e^2 \hbar}{V} \sum_{mn} f(\varepsilon_n) \frac{(v_{nm}^\alpha v_{mn}^\beta - v_{nm}^\beta v_{mn}^\alpha)}{(\varepsilon_n - \varepsilon_m)^2 + \left(\frac{\hbar}{\tau}\right)^2}. \quad (\text{D5})$$

The equilibrium value for the Hall conductivity for  $\tau \rightarrow \infty$  is hence obtained as

$$\sigma_H = \frac{i e^2 \hbar}{V} \sum_{mn} f(\varepsilon_n) \frac{(v_{nm}^\alpha v_{mn}^\beta - v_{nm}^\beta v_{mn}^\alpha)}{(\varepsilon_n - \varepsilon_m)^2}, \quad (\text{D6})$$

which describes the thermally averaged Berry curvature [20,36]. Using the spectral-projection operator, we obtain the Hall conductivity as

$$\sigma_H = \frac{i e^2 \hbar}{V} \int_{-\infty}^{\infty} dE f(E) \text{Tr} \times \left[ \delta(E - \hat{H}) \left( \hat{v}_\alpha \frac{1}{(E - \hat{H})^2} \hat{v}_\beta - \text{H.c.} \right) \right]. \quad (\text{D7})$$

Thus the equilibrium value of the dc conductivity can equivalently be written as

$$\sigma_{\alpha\beta} = -\frac{e^2 \pi \hbar}{V} \int_{-\infty}^{\infty} dE \frac{df(E)}{dE} \text{Tr}[\delta(E - \hat{H}) \hat{v}_\alpha \delta(E - \hat{H}) \hat{v}_\beta] + \sigma_H, \quad (\text{D8})$$

which we derived directly from Eq. (1).

## APPENDIX E: RELATION OF THE dc CONDUCTIVITY TO THE KUBO-BASTIN FORMULA

In this Appendix, we show the equivalence of the dc conductivity used in this work with the Kubo-Bastin formula [43] based on the equilibrium values of the symmetric and the antisymmetric parts of the dc conductivity derived in Appendix D. We start with the symmetric part of the conductivity and discuss its relation to the Kubo-Bastin formula. For this purpose, we introduce the Green's functions

$$\hat{G}^\pm(E) = \lim_{\eta \rightarrow 0} \frac{1}{E - \hat{H} \pm i\eta} = \lim_{\tau \rightarrow \infty} \frac{1}{E - \hat{H} \pm \frac{i\hbar}{\tau}}, \quad (\text{E1})$$

where the real and the imaginary parts are given by

$$\text{Re} \hat{G}(E) = \frac{1}{E - \hat{H}} = \lim_{\tau \rightarrow \infty} \frac{E - \hat{H}}{(E - \hat{H})^2 + \left(\frac{\hbar}{\tau}\right)^2}, \quad (\text{E2})$$

$$\text{Im} \hat{G}(E) = -\pi \delta(E - \hat{H}) = -\lim_{\tau \rightarrow \infty} \frac{\frac{\hbar}{\tau}}{(E - \hat{H})^2 + \left(\frac{\hbar}{\tau}\right)^2}. \quad (\text{E3})$$

The Kubo-Bastin formula for the Hall conductivity reads [43]

$$\sigma_{\alpha\beta}^{\text{Bastin}} = \frac{e^2}{V} \int_{-\infty}^{\infty} dE f(E) C_{\alpha\beta}(E), \quad (\text{E4})$$

with  $f(E)$  being the Fermi function and  $C_{\alpha\beta}(E)$  being the correlation function

$$C_{\alpha\beta}(E) = i\hbar \text{Tr} \left[ \hat{v}_\alpha \delta(E - \hat{H}) \hat{v}_\beta \frac{d\hat{G}^+(E)}{dE} - \text{H.c.} \right]. \quad (\text{E5})$$

To prove the equivalence to the present version of the dc conductivity based on Eq. (1), we may decompose  $C_{\alpha\beta}(E)$  as follows:

$$C_{\alpha\beta}(E) = C_{\alpha\beta}^s(E) + C_{\alpha\beta}^{\text{as}}(E), \quad (\text{E6})$$

with  $C_{\alpha\beta}^{\text{as}}(E) = [C_{\alpha\beta}(E) + (-)C_{\beta\alpha}(E)]/2$  yielding

$$C_{\alpha\beta}^s(E) = \pi \hbar \frac{d}{dE} \text{Tr}[\delta(E - \hat{H}) \hat{v}_\alpha \delta(E - \hat{H}) \hat{v}_\beta], \quad (\text{E7})$$

$$C_{\alpha\beta}^{\text{as}}(E) = i\hbar \text{Tr} \left[ \delta(E - \hat{H}) \left( \hat{v}_\alpha \frac{1}{(E - \hat{H})^2} \hat{v}_\beta - \text{H.c.} \right) \right], \quad (\text{E8})$$

which can be proven straightforwardly. Consequently, we find for the dc conductivity

$$\sigma_{\alpha\beta}^{\text{Bastin}} = \frac{e^2 \pi \hbar}{V} \int_{-\infty}^{\infty} dE f(E) \frac{d}{dE} \times \text{Tr}[\delta(E - \hat{H}) \hat{v}_\alpha \delta(E - \hat{H}) \hat{v}_\beta] + \sigma_H, \quad (\text{E9})$$

where the Hall conductivity is obtained from the antisymmetric term  $C_{\alpha\beta}^{\text{as}}(E)$  in the Kubo-Bastin formula. Using integration by parts for the energy integral involving  $C_{\alpha\beta}^{\text{as}}(E)$  in the Kubo-Bastin formula, we readily obtain the equilibrium value of the dc conductivity of Eq. (D8),

$$\begin{aligned}\sigma_{\alpha\beta}^{\text{Bastin}} &= \sigma_{\alpha\beta}^{\text{s}} + \sigma_{\text{H}} \\ &= \sigma_{\alpha\beta},\end{aligned}\quad (\text{E10})$$

which is equivalent to Eq. (1) in the limit  $\tau \rightarrow \infty$ . We furthermore can split the antisymmetric term  $C_{\alpha\beta}^{\text{as}}$  into two terms yielding

$$\begin{aligned}C_{\alpha\beta}^{\text{as}} &= -\frac{1}{2}\text{Tr}\left[\frac{d}{dE}\delta(E - \hat{H})(\hat{v}_{\alpha}\hat{x}_{\beta} - \hat{v}_{\beta}\hat{x}_{\alpha})\right] \\ &+ \text{Tr}[\delta(E - \hat{H})(\hat{v}_{\alpha}[\text{Re}\hat{G}(E), \hat{x}_{\beta}] + \text{H.c.})].\end{aligned}\quad (\text{E11})$$

Hence the Hall conductivity is decomposed into

$$\sigma_{\text{H}} = \sigma_{\text{H}}^{\text{I}} + \sigma_{\text{H}}^{\text{II}},\quad (\text{E12})$$

with

$$\begin{aligned}\sigma_{\text{H}}^{\text{I}} &= \frac{e^2}{2V}\int_{-\infty}^{\infty}dE f(E)\text{Tr}[\delta(E - \hat{H}) \\ &\times (\hat{v}_{\alpha}[\text{Re}\hat{G}(E), \hat{x}_{\beta}] + \text{H.c.})],\end{aligned}\quad (\text{E13})$$

$$\sigma_{\text{H}}^{\text{II}} = \frac{e^2}{2V}\int_{-\infty}^{\infty}dE f(E)\text{Tr}\left[\frac{d}{dE}\delta(E - \hat{H})(\hat{x}_{\alpha}\hat{v}_{\beta} - \hat{x}_{\beta}\hat{v}_{\alpha})\right].\quad (\text{E14})$$

We note that  $\sigma_{\text{H}}^{\text{II}}$  also appears in the Středa formula [44]. The above decomposition of the Hall conductivity can be used to prove Eq. (21) (see Appendix C), i.e., the semiclassical result for the Hall conductivity.

## APPENDIX F: MATERIAL PARAMETERS OF THE EFFECTIVE POLARON MODEL WITH VIBRATIONAL DISORDER

In Table I, we summarize the material parameters for the electronic coupling and the vibrational disorder (at 140 K and at 300 K) entering the effective polaron Hamiltonian in Eq. (14) of the main text.

TABLE I. Summary of material parameters used in the effective polaron Hamiltonian in Eq. (14). The values for the vibrational disorder are shown for the highest and for the lowest temperatures that have been investigated throughout this study. The molecular parameters for the electronic transfer integrals and the vibrational disorder are based on an *ab initio* study of the electron-phonon coupling in rubrene [48].

Material parameter	Value (meV)
On-site energy	0.0
$\varepsilon_{\text{AA+b}}$	134.0
$\varepsilon_{\text{AA+2b}}$	-10.7
$\varepsilon_{\text{AC}}$	28.6
$\varepsilon_{\text{AB}}$	4.1
$V_0^{300\text{ K}}$	52.1
$V_{\text{AA+b}}^{300\text{ K}}$	20.9
$V_{\text{AA+2b}}^{300\text{ K}}$	0.0
$V_{\text{AC}}^{300\text{ K}}$	8.7
$V_{\text{AB}}^{300\text{ K}}$	0.9
$V_0^{140\text{ K}}$	48.2
$V_{\text{AA+b}}^{140\text{ K}}$	15.1
$V_{\text{AA+2b}}^{140\text{ K}}$	0.0
$V_{\text{AC}}^{140\text{ K}}$	6.3
$V_{\text{AB}}^{140\text{ K}}$	0.6

- [1] K. von Klitzing, T. Chakraborty, P. Kim, V. Madhavan, X. Dai, J. McIver, Y. Tokura, L. Savary, D. Smirnova, A. M. Rey, C. Felser, J. Gooth, and X. Qi, 40 years of the quantum Hall effect, *Nat. Rev. Phys.* **2**, 397 (2020).
- [2] V. Podzorov, E. Menard, J. A. Rogers, and M. E. Gershenson, Hall effect in the accumulation layers on the surface of organic semiconductors, *Phys. Rev. Lett.* **95**, 226601 (2005).
- [3] B. Lee, Y. Chen, D. Fu, H. T. Yi, K. Czelen, H. Najafov, and V. Podzorov, Trap healing and ultralow-noise Hall effect at the surface of organic semiconductors, *Nat. Mater.* **12**, 1125 (2013).
- [4] W. Xie, K. A. McGarry, F. Liu, Y. Wu, P. P. Ruden, C. J. Douglas, and C. D. Frisbie, High-mobility transistors based on single crystals of isotopically substituted rubrene-d<sub>28</sub>, *J. Phys. Chem. C* **117**, 11522 (2013).
- [5] W. Xie, S. Wang, X. Zhang, C. Leighton, and C. D. Frisbie, High conductance 2D transport around the Hall mobility peak in electrolyte-gated rubrene crystals, *Phys. Rev. Lett.* **113**, 246602 (2014).
- [6] Y. Chen, H. T. Yi, and V. Podzorov, High-resolution ac measurements of the Hall effect in organic field-effect transistors, *Phys. Rev. Appl.* **5**, 034008 (2016).
- [7] H. T. Yi, Y. N. Gartstein, and V. Podzorov, Charge carrier coherence and Hall effect in organic semiconductors, *Sci. Rep.* **6**, 23650 (2016).
- [8] H. H. Choi, K. Cho, C. D. Frisbie, H. Sirringhaus, and V. Podzorov, Critical assessment of charge mobility extraction in FETs, *Nat. Mater.* **17**, 2 (2018).
- [9] H. H. Choi, A. F. Paterson, M. A. Fusella, J. Panidi, O. Solomeshch, N. Tessler, M. Heeney, K. Cho, T. D. Anthopoulos, B. P. Rand, and V. Podzorov, Hall effect in polycrystalline organic semiconductors: The effect of grain boundaries, *Adv. Funct. Mater.* **30**, 1903617 (2020).
- [10] C. Lee, T. Schiros, E. J. G. Santos, B. Kim, K. G. Yager, S. J. Kang, S. Lee, J. Yu, K. Watanabe, T. Taniguchi, J. Hone, E. Kaxiras, C. Nuckolls, and P. Kim, Epitaxial growth of molecular crystals on van der Waals substrates for high-performance organic electronics, *Adv. Mater.* **26**, 2812 (2014).

- [11] J.-F. Chang, T. Sakanoue, Y. Olivier, T. Uemura, M.-B. Dufourg-Madec, S. G. Yeates, J. Cornil, J. Takeya, A. Troisi, and H. Siringhaus, Hall-effect measurements probing the degree of charge-carrier delocalization in solution-processed crystalline molecular semiconductors, *Phys. Rev. Lett.* **107**, 066601 (2011).
- [12] T. Uemura, M. Yamagishi, J. Soeda, Y. Takatsuki, Y. Okada, Y. Nakazawa, and J. Takeya, Temperature dependence of the Hall effect in pentacene field-effect transistors: Possibility of charge decoherence induced by molecular fluctuations, *Phys. Rev. B* **85**, 035313 (2012).
- [13] N. A. Minder, S. Ono, Z. Chen, A. Facchetti, and A. F. Morpurgo, Band-like electron transport in organic transistors and implication of the molecular structure for performance optimization, *Adv. Mater.* **24**, 503 (2012).
- [14] M. Yamagishi, J. Soeda, T. Uemura, Y. Okada, Y. Takatsuki, T. Nishikawa, Y. Nakazawa, I. Doi, K. Takimiya, and J. Takeya, Free-electron-like Hall effect in high-mobility organic thin-film transistors, *Phys. Rev. B* **81**, 161306(R) (2010).
- [15] S. Fratini, M. Nikolka, A. Salleo, G. Schweicher, and H. Siringhaus, Charge transport in high-mobility conjugated polymers and molecular semiconductors, *Nat. Mater.* **19**, 491 (2020).
- [16] N. Kasuya, J. Tsurumi, T. Okamoto, S. Watanabe, and J. Takeya, Two-dimensional hole gas in organic semiconductors, *Nat. Mater.* **20**, 1401 (2021).
- [17] K. von Klitzing, The quantized Hall effect, *Rev. Mod. Phys.* **58**, 519 (1986).
- [18] Y. Zhang, Y. Tan, H. L. Stormer, and P. Kim, Experimental observation of the quantum Hall effect and Berry's phase in graphene, *Nature (London)* **438**, 201 (2005).
- [19] K. S. Novoselov, Z. Jiang, Y. Zhang, S. V. Morozov, H. L. Stormer, U. Zeitler, J. C. Maan, G. S. Boebinger, P. Kim, and A. K. Geim, Room-temperature quantum Hall effect in graphene, *Science* **315**, 1379 (2007).
- [20] D. J. Thouless, M. Kohmoto, M. P. Nightingale, and M. den Nijs, Quantized Hall conductance in a two-dimensional periodic potential, *Phys. Rev. Lett.* **49**, 405 (1982).
- [21] F. D. M. Haldane, Model for a quantum Hall effect without Landau levels: Condensed-matter realization of the "parity anomaly", *Phys. Rev. Lett.* **61**, 2015 (1988).
- [22] C. L. Kane and E. J. Mele, Quantum spin Hall effect in graphene, *Phys. Rev. Lett.* **95**, 226801 (2005).
- [23] H. Ishii, H. Tamura, M. Tsukada, N. Kobayashi, and K. Hirose, Large-scale conductivity-tensor calculations for Hall effects in time-dependent wave-packet diffusion method, *Phys. Rev. B* **90**, 155458 (2014).
- [24] Z. G. Yu, Spin Hall effect in disordered organic solids, *Phys. Rev. Lett.* **115**, 026601 (2015).
- [25] M. V. Berry, Quantal phase factors accompanying adiabatic changes, *Proc. Math. Phys. Eng. Sci.* **392**, 45 (1984).
- [26] S. Ponc e, F. Macheda, E. R. Margine, N. Marzari, N. Bonini, and F. Giustino, First-principles predictions of Hall and drift mobilities in semiconductors, *Phys. Rev. Res.* **3**, 043022 (2021).
- [27] S. Fratini, D. Mayou, and S. Ciuchi, The transient localization scenario for charge transport in crystalline organic materials, *Adv. Funct. Mater.* **26**, 2292 (2016).
- [28] S. Fratini, S. Ciuchi, D. Mayou, G. T. De Laissardi ere, and A. Troisi, A map of high-mobility molecular semiconductors, *Nat. Mater.* **16**, 998 (2017).
- [29] S. Hutsch, M. Panhans, and F. Ortmann, Charge carrier mobilities of organic semiconductors: ab initio simulations with mode-specific treatment of molecular vibrations, *npj Comput. Mater.* **8**, 228 (2022).
- [30] L. Friedman and M. Pollak, The Hall effect in the variable-range-hopping regime, *Philos. Mag. B* **44**, 487 (1981).
- [31] A. V. Shumilin and N. P. Stepina, Hall effect in two-dimensional systems with hopping transport and strong disorder, *Phys. Rev. B* **98**, 115303 (2018).
- [32] H. Oberhofer, K. Reuter, and J. Blumberger, Charge transport in molecular materials: An assessment of computational methods, *Chem. Rev.* **117**, 10319 (2017).
- [33] M. Panhans and F. Ortmann, Efficient time-domain approach for linear response functions, *Phys. Rev. Lett.* **127**, 016601 (2021).
- [34] R. Kubo, Statistical-mechanical theory of irreversible processes. I. General theory and simple applications to magnetic and conduction problems, *J. Phys. Soc. Jpn.* **12**, 570 (1957).
- [35] L. Landau, Diamagnetismus der Metalle, *Z. Phys.* **64**, 629 (1930).
- [36] Q. Niu, D. J. Thouless, and Y.-S. Wu, Quantized Hall conductance as a topological invariant, *Phys. Rev. B* **31**, 3372 (1985).
- [37] M. Kohmoto, Topological invariant and the quantization of the Hall conductance, *Ann. Phys. (NY)* **160**, 343 (1985).
- [38] L. Onsager, Reciprocal relations in irreversible processes. I., *Phys. Rev.* **37**, 405 (1931).
- [39] H. B. G. Casimir, On onsager's principle of microscopic reversibility, *Rev. Mod. Phys.* **17**, 343 (1945).
- [40] R. Luo, G. Benenti, G. Casati, and J. Wang, Onsager reciprocal relations with broken time-reversal symmetry, *Phys. Rev. Res.* **2**, 022009(R) (2020).
- [41] Z. Fan, J. H. Garcia, A. W. Cummings, J. E. Barrios-Vargas, M. Panhans, A. Harju, F. Ortmann, and S. Roche, Linear scaling quantum transport methodologies, *Phys. Rep.* **903**, 1 (2021).
- [42] D. A. Greenwood, The Boltzmann equation in the theory of electrical conduction in metals, *Proc. Phys. Soc.* **71**, 585 (1958).
- [43] A. Bastin, C. Lewiner, O. Betbeder-matibet, and P. Nozieres, Quantum oscillations of the Hall effect of a fermion gas with random impurity scattering, *J. Phys. Chem. Solids* **32**, 1811 (1971).
- [44] P. Streda, Theory of quantised Hall conductivity in two dimensions, *J. Phys. C: Solid State Phys.* **15**, L717 (1982).
- [45] J. H. Garc a, L. Covaci, and T. G. Rappoport, Real-space calculation of the conductivity tensor for disordered topological matter, *Phys. Rev. Lett.* **114**, 116602 (2015).
- [46] J. Mitscherling, Longitudinal and anomalous Hall conductivity of a general two-band model, *Phys. Rev. B* **102**, 165151 (2020).
- [47] S. G. de Castro, J. M. V. P. Lopes, A. Ferreira, and D. A. Bahamon, Fast fourier-chebyshev approach to real-space simulations of the kubo formula, *Phys. Rev. Lett.* **132**, 076302 (2024).
- [48] P. Ordej on, D. Boskovic, M. Panhans, and F. Ortmann, *Ab initio* study of electron-phonon coupling in rubrene, *Phys. Rev. B* **96**, 035202 (2017).
- [49] K. Hannewald, V. M. Stojanovi c, J. M. T. Schellekens, P. A. Bobbert, G. Kresse, and J. Hafner, Theory of polaron bandwidth narrowing in organic molecular crystals, *Phys. Rev. B* **69**, 075211 (2004).

- [50] F. Ortmann, F. Bechstedt, and K. Hannewald, Theory of charge transport in organic crystals: Beyond Holstein's small-polaron model, *Phys. Rev. B* **79**, 235206 (2009).
- [51] K. Merkel, M. Panhans, S. Hutsch, and F. Ortmann, Interplay of band occupation, localization, and polaron renormalization for electron transport in molecular crystals: Naphthalene as a case study, *Phys. Rev. B* **105**, 165136 (2022).
- [52] J. M. Luttinger, The effect of a magnetic field on electrons in a periodic potential, *Phys. Rev.* **84**, 814 (1951).
- [53] N. W. Ashcroft and N. D. Mermin, *Solid State Physics*, HRW International Editions (Holt, Rinehart, and Winston, New York, 1976).
- [54] I. M. Lifshitz, M. Azbel, and M. Kaganov, The theory of galvanomagnetic effects in metals, *Sov. Phys. JETP* **4**, 41 (1957).
- [55] M. Arai and Y. Hatsugai, Quantum Hall effects of graphene with multiorbitals: Topological numbers, Boltzmann conductance, and semiclassical quantization, *Phys. Rev. B* **79**, 075429 (2009).
- [56] I. M. Lifshitz, Anomalies of electron characteristics of a metal in the high pressure region, *Sov. Phys. JETP* **11**, 1130 (1960).
- [57] A. S. Mishchenko, N. Nagaosa, G. De Filippis, A. de Candia, and V. Cataudella, Mobility of Holstein polaron at finite temperature: An unbiased approach, *Phys. Rev. Lett.* **114**, 146401 (2015).
- [58] A. S. Mishchenko, L. Pollet, N. V. Prokof'ev, A. Kumar, D. L. Maslov, and N. Nagaosa, Polaron mobility in the "beyond quasiparticles" regime, *Phys. Rev. Lett.* **123**, 076601 (2019).
- [59] Z. Zhu, J. Wang, H. Zuo, B. Fauqué, R. D. McDonald, Y. Fuseya, and K. Behnia, Emptying Dirac valleys in bismuth using high magnetic fields, *Nat. Commun.* **8**, 15297 (2017).
- [60] D. N. Sheng and Z. Y. Weng, Disappearance of integer quantum Hall effect, *Phys. Rev. Lett.* **78**, 318 (1997).
- [61] K. Yang and R. N. Bhatt, Floating of extended states and localization transition in a weak magnetic field, *Phys. Rev. Lett.* **76**, 1316 (1996).
- [62] D. Z. Liu, X. C. Xie, and Q. Niu, Weak field phase diagram for an integer quantum Hall liquid, *Phys. Rev. Lett.* **76**, 975 (1996).
- [63] P. Danielewicz, Quantum theory of nonequilibrium processes, I, *Ann. Phys. (NY)* **152**, 239 (1984).